Heinrich Heine Universität Düsseldorf

Adaptively measuring quantum expectation values using the empirical Bernstein stopping rule

Bachelorarbeit

am Institut für theoretische Physik, Düsseldorf
vorgelegt von

Ugur Tepe

Matrikelnummer: 2724342

Erstprüfer
Prof. Dr. Martin Kliesch
Institute for Quantum Inspired and Quantum Optimization
Hamburg University of Technology

Zweitprüfer:
Prof. Dr. Dagmar Bruß
Institut für theoretische Physik III
Heinrich-Heine-Universität Düsseldorf

27.11.2023

Abstract

Quantum computing promises to be exponentially faster than classical computers, in a wide array of computational tasks. These tasks range from solving combinatorial problems or systems of equations in mathematics to simulating complex physical systems. Especially for simulating physical systems, quantum computers are thought to excel.
Although promising, a general quantum advantage over classical computers is yet to be achieved. A quantum advantage refers to a point at which quantum computers can solve complex problems that classical computers cannot solve in a finite amount of time. The current generation of quantum computers, also known as noisy intermediate scale quantum (NISQ) quantum devices, are restricted by noise. As a consequence they are limited in the number of qubits and noise Methods are developed to make the best out of the currently available hardware. Hence, these methods must deal with quantum errors, limited circuit depths, and limited qubit numbers.
A popular method are the so-called variational quantum algorithms (VQA), which employ a optimisation-based approach. VQAs employ parameterised quantum circuits, whose parameters are optimised on a classical computer.
However, VQAs face a multitude of problems, one of them being the required measurement effort in order to yield accurate results.
The goal of this thesis is to show that the measurement effort in VQAs can be reduced by the so-called empirical Bernstein stopping (EBS) algorithm. EBS provides an estimate with an accuracy guarantee Reducing the measurement effort is, however, not a unique problem of VQAs and therefore the results of this thesis will be applicable to a wider array of quantum algorithms.

Contents

1. Introduction

Although the current generation of quantum computers can exceed classical computers in tasks specifically designed for available quantum hardware [2, 3], a practical quantum advantage is yet to be achieved. Thus, the goal is to utilise the available hardware, often referred to as noisy intermediate scale quantum era (NISQ) hardware, to achieve said advantage over classical computers. These NISQ quantum computers are limited in the number of qubits and are subject to noise. The latter effectively restricts the total length of the computation as well as the total number of operations used.
Fault-tolerant (FT) quantum computers are the solution for the noise problem, however, they require more qubits than currently available. Additionally, adding more qubits and increasing circuit depth to implement FT quantum computers also increases noise.
Variational quantum algorithms (VQAs) are a popular approach to employ the current generations of quantum hardware. These algorithms are designed to designed to obey the limited circuit depth and qubit numbers. The key idea behind VQAs is to utilise classical computers that interface with the quantum computer via the parameters of a parameterised quantum circuit. In particular, these parameters are optimised using classical optimisation techniques, e.g. a gradient-based one. These parameters are tuned such that the cost function is minimised. The cost function can be, for example, the expected energy of the Hamiltonian as a function of some parameter(s). This is possible due to the variational principle, which states that any measured energy is always above the ground energy. Thus optimising towards the ground energy is effective in finding the ground state or any other minima.
Naturally, such methods can be used to solve problems from quantum chemistry or problems of combinatorial nature [4]. However, these VQAs face several issues:

- The optimisation process can get stuck in a barren plateau or local minima [5, 6],
- The sample effort for the read-out of the algorithm can bottleneck the VQA [4, 7],
- In general, finding a suitable parametrized circuit (often referred to as the ansatz) is hard. [8].

Barren plateaus are regions in the cost landscape where the expected gradient goes to zero with increased system size, causing the optimiser to get stuck. A similar problem can be encountered in local minima as the gradient vanishes there as well. For the barren plateau problem there are multiple suggested techniques to avoid them [9–11]. Especially in quantum chemistry problems, a certain accuracy is required which results in a sample bottleneck as naturally one wants to also minimise the amounts of samples that are required for an accurate estimate Such estimates are produced using so-called stopping algorithm, which guarantee an accuracy and confidence. They determine when to stop sampling according to a specified conditions, e.g., the accuracy of the current estimate.
One such algorithm is the empirical Bernstein stopping (EBS) algorithm. Stopping rules, like EBS, manage how many samples are needed to estimate

the mean of a series of i.i.d random variables. This estimate is called an (ϵ, δ)-estimate, as it is within ϵ of the actual mean, with the probability of at least $1 - \delta$. In contrast to similar stopping rules, EBS incorporates the empirical variance, which is estimated as well, into its stopping condition. Hence, EBS is called an adaptive stopping rule, as it is dependent on the explicit samples drawn. The goal of this thesis is to test whether EBS decrease the sample requirements for quantum algorithms such as VQAs. EBS performs well especially when the variance of the random variable is low compared to their range. VQAs provide a wide array of variance regimes, as near a minima or saddle point the variance vanishes while increasing in other regions. As the overarching goal of VQAs is to to estimate the ground energy, EBS may provide a significant improvement compared to usual methods, as it benefits from the vanishing variance. Over a VQE optimisation run, this may lead to a more efficient sampling strategy.

2. Preliminaries

This section serves as a quick primer on topics such as probability theory, quantum mechanics and quantum computing. Firstly a refresher on probability theory is given, as concepts like random variables and expected values are a key concepts in this thesis. Further, probability theory is needed to introduce the concept of concentration inequalities, on which the empirical Bernstein stopping algorithm is based on.
Secondly quantum mechanics serves as a foundation to quantum computing, where concepts as qubits, gates and circuits are introduced as well as variational quantum algorithms.

2.1. Probability Theory

This section provides a refresher of the basics of probability theory. Probability theory is a fundamental component of quantum mechanics, quantum information. Along side the basics of probability theory, this section also introduces the concept of tail bounds, starting with the most fundamental one. Tail bounds are a important conceptual tool to understand as they are employed by stopping algorithms which are introduced and discussed in later sections of this thesis.

2.1.1. Random Variables

A random variable X is a function that maps from an (unknown) probability space S to a real number $\mathbb{R}$ [12].

$$X : S \to \mathbb{R} \tag{1}$$

Random variables can be continuous or discrete, however in this thesis only discrete random variables are of importance. The randomness of the random variable is tied to the random experiment they come from. For example, in the case of a dice, the trivial random variable looks like:

$$x(1) = 1, \quad x(2) = 2, \quad x(3) = 3, \quad x(4) = 4, \quad x(5) = 5, \quad x(6) = 6 \tag{2}$$

with $X = \{x(i)\}$ and $i = \{1, 2, \ldots, 6\}$.
Each random variable x_i occurs with a probability of $1/6$ and has the value of the corresponding dice number.
Another example would be to divide the outcomes of the dice into odd and even facing numbers. This would result in the corresponding random variable only having 2 values, **odd** or **even**:

$$x(\text{odd}) = -1 \qquad x(\text{even}) = 1 \tag{3}$$

with $X = \{x(\text{odd}), x(\text{even})\}$.
Each of these two random variables has the associated probability of $1/2$ and discrete number, 1 or -1, mapped to them.
When a collection of identical random variables is considered, and it is assumed that each one is independent of the other, they are called independent and identically distributed random variables (i.i.d.).
Multiple dice throws, for example, are i.i.d. random variables.

2.1.2. Expectation Value

The expected value of a random variable is the average of every outcome that can occur multiplied by its probability density. It is also known as the first moment (because X only goes in linearly).
In the discrete case, it is defined as:

$$\mathbb{E}[X] = \langle X \rangle = \mu = \sum_i x_i p_i, \tag{4}$$

with p_i being the probability of x_i.
Of course calculating the expected value like this is not always possible as the probability distribution is usually unknown, to that extend one can use the so called empirical mean. The aforementioned is calculated as follows:

$$\bar{X} = \frac{1}{N} \sum_{i=1}^{N} X_i \, . \tag{5}$$

2.1.3. Variance

The variance measures how much the random variable may vary from its expected value. The variance of a random variable X is the expected squared deviation from its expected value $\mathbb{E}[X] = \mu$:

$$\mathrm{Var}(X) = \mathbb{E}\left[(X-\mu)^2\right] = \mathbb{E}\left[X^2\right] - \mathbb{E}\left[X\right]^2 . \tag{6}$$

For a discrete random variable X, assuming the probabilities are known, its variance can be calculated as:

$$\mathrm{Var}(X) = \sum_i p_i (x_i - \mu)^2 . \tag{7}$$

In many applications it is not possible to access the probabilities p_i to calculate the variance. For these cases, there is the so-called (unbiased) **sample variance** Var_s. Like the name suggests, the sample variance is calculated from N samples:

$$\mathrm{Var}_s(X) = \frac{1}{N-1} \sum_{i=1}^{N} (x_i - \bar{X})^2, \tag{8}$$

with $\bar{X}$ being the empirical mean.
Closely related to the variance is the **standard deviation** σ

$$\sigma = \sqrt{\mathrm{Var}(X)} \, . \tag{9}$$

Hence, the variance is also commonly denoted as σ^2.
The variance of a bounded probability distribution can be bounded using Popoviciu's inequality [13]:

$$0 \leq \sigma^2 \leq \frac{R^2}{4} . \tag{10}$$

2.2. Concentration Inequalities

When considering a series of random variables it may be of use to determine how far they deviate from their expected value based on the number of samples. It is clear that the empirical mean of this sequence converges to the actual mean or expected value, based on how many samples are drawn. Often it is of interest to know when the empirical mean is converged such that it is within a constant from the actual mean. This convergence can be characterised using so called **concentration inequalities**. These inequalities vary in how tightly they bound the tail and the restrictions imposed on the random variables. The most fundamental inequality is Markov's, it assumes only that the random variables are almost surely non-negative[1]. Markov's inequality serves as an introduction to more advanced inequalities like Bernstein's inequality and Höffding's inequality are also introduced.

2.2.1. Markov's Inequality

Let X be an almost surely non-negative random variable and $\epsilon > 0$, then Markov's inequality is as follows:

$$\mathbb{P}[X \geq \epsilon] \leq \frac{\mathbb{E}[X]}{\epsilon}. \tag{11}$$

With this inequality the upper bound to probabilities of various events can be calculated, e.g. how likely it is at most to roll a dice that is greater or equal to a 4.

$$\mathbb{P}[X \geq 4] \leq \frac{3.5}{4} = 0.875. \tag{12}$$

The 87.5% is only a crude upper bound for the probability. Compared to the actual probability $\mathbb{P}[X \geq 4] = 50\%$, the upper bound provided by Markov's inequality is substantially larger. This discrepancy is due to the fact that Markov's inequality assumes only that the random variables are almost surely non-negative. If more assumptions are made, or even more empirical information is taken into account, these bounds can be improved significantly. The subject of the following sub-section are such methods.

2.2.2. Höffding's Inequality

An inequality frequently used for stopping algorithms, e.g., in machine learning or quantum computing, is Höffding's inequality [14]. Höffding's inequality gives a bound on how much the mean of a series of random variables deviates from its expected value μ. This bound depends on their range R and the number of samples t taken.
Let $X_1, ..., X_t$ be independent random variables with $a_i \leq X_i \leq b_i$ and $\overline{X}_t = \frac{1}{t}\sum_{i=1}^{t} X_i$, Höffding's inequality [15] is as follows:

$$\mathbb{P}[|\overline{X}_t - \mu| \geq \epsilon] \leq 2\exp\left(-\frac{2(t\epsilon)^2}{\sum_{i=1}^{t}(b_i - a_i)^2}\right). \tag{13}$$

[1]Almost surely non-negative random variables are random variables that fulfil: $\mathbb{P}[X \geq 0] = 1$. This means they can take negative values, but with the probability of 0 to occur.

If all X_i are bounded by the same interval $[a_i, b_i]$ with the range $R = b - a$. equation (13) simplifies to:

$$\mathbb{P}[|\overline{X}_t - \mu| \geq \epsilon] \leq 2\exp\left(-\frac{2t\epsilon^2}{R^2}\right) =: \delta, \tag{14}$$

with $\sum_{i=1}^{t}(b_i - a_i)^2 = tR^2$ and defining the left hand side as δ.
δ is the probability that after t many samples, the empirical mean deviates at-least ϵ from the actual mean. This inequality can be rearranged to a bound form [16], which is more suitable to quantify the current accuracy of the estimate:

$$|\overline{X}_t - \mu| \leq R\sqrt{\frac{\ln(2/\delta)}{2t}}. \tag{15}$$

This inequality holds with probability of at-least $1 - \delta$. Since Höffding's inequality depends only on the range R, we can set the right-hand side of eq. (15) equal to a desired accuracy ϵ and confidence $1 - \delta$ and solve for t.

$$t_{\min} := 2\left(\frac{R}{\epsilon}\right)^2 \ln(2/\delta). \tag{16}$$

$t_{\min}$ is also referred to as the sample complexity of the random variable, as it determines how many samples are needed to obtain an estimate that is within ϵ, $1 - \delta$ of the time. This concept of having an estimate, characterized by the two parameters ϵ and δ is called a (ϵ, δ) estimate and will be discussed in a later section in more detail.

2.2.3. Bernstein's Inequality

Similar to Höffding's inequality, Bernstein's inequality also bounds the sum of random variables. The key difference is that unlike Höffding's inequality, Bernstein's is dependent on the variance of the random variables as well. Let $X_1, ..., X_t$ be i.i.d. random variables with range R, expected value μ, and variance σ^2 each.
Let $\overline{X}_t = \frac{1}{t}\sum_{i=1}^{t} X_i$ and $\Sigma^2 = \sum_{i=1}^{t}\sigma_i^2$. Then, Bernstein's inequality [15] is as follows:

$$\mathbb{P}[|\overline{X}_t - \mu| \geq \epsilon] \leq 2\exp\left(-\frac{(t\epsilon)^2/2}{\Sigma^2 + Rt\epsilon/3}\right) \overset{!}{=} \delta. \tag{17}$$

Like with Höffding's inequality, it is beneficial to rewrite the inequality into a bounded form. The derivation of this bound can be found in appendix A and yields:

$$|\overline{X}_t - \mu| \leq \sigma\underbrace{\sqrt{\frac{2\ln(2/\delta)}{t}}}_{\mathcal{O}(1/\sqrt{t})} + \underbrace{\frac{R\ln(2/\delta)}{3t}}_{\mathcal{O}(1/t)}. \tag{18}$$

Because the variance is unknown in practical scenarios (such as the underlying distribution), the variance in equation (18) has to be replaced [17] by the empirical standard deviation $\overline{\sigma}_t = \sqrt{\frac{1}{t}\sum_{i=1}^{t}(X_i - \overline{X}_t)^2}$. This yields empirical form of eq. (18):

$$|\overline{X}_t - \mu| \leq \overline{\sigma}_t\sqrt{\frac{2\ln(3/\delta)}{t}} + \frac{3R\ln(3/\delta)}{t}. \tag{19}$$

A proof of the inequality and bound can be found in [17]. The fact that the variance can be replaced with an estimated variance in Bernstein's bound is a surprising and profound statement. This result makes it possible to use Bernstein's bound in cases where the probability distribution and the corresponding variance is not known.
In the following section, the previously introduced bounds of Bernstein and Höffding are quickly compared with each other.

2.2.4. Höffding's vs. Bernstein's Inequality

To better understand in which scenarios Bernstein's bound is advantageous over Höffding's bound, it is useful to compare the inequalities. In the empirical Bernstein bound (18), the term with the empirical standard deviation or the empirical variance decreases with $1/\sqrt{t}$ while the term with the range R decreases with $1/t$, rendering the term that involves the range negligible for large t. If the standard deviation is substantially smaller than the range, Bernstein's bound becomes much tighter than Höffding's bound for larger t. In this case the remaining term both decrease with $\mathcal{O}(1/\sqrt{t})$. Hence, the advantage of one bound over the other depends on whether $\sigma \ll R$ is fulfilled.

$$|\overline{X}_t - \mu| \leq \sigma\sqrt{\frac{2\ln(3/\delta)}{t}} + \frac{R\ln(2/\delta)}{3t} \qquad \text{(Bernstein's Bound)} \tag{20}$$

$$|\overline{X}_t - \mu| \leq R\sqrt{\frac{\ln(2/\delta)}{2t}} \qquad \text{(Höffding's Bound)} \tag{21}$$

with δ fixed to 0.1.
We plot the comparison of the two bounds (20) & (21) as a function of the sample number t, the range R and the variance σ^2 in figure 1. Note that the variance of any bounded probability distribution is bounded by $R^2/4$, see eq. (10). Hence, for a range of $R = 2$ the maximally possible variance is $\sigma^2 = 1$, which is the worst-case for Bernstein's bound. Consequently, Höffding's bound is seen to be tighter than Bernstein's bound in said worst-case, in figure 1. However, Bernstein's bound remained tighter for larger t, for the remaining cases. Additionally, we observe that Höffding's bound does not depend on σ^2, hence does not benefit from decreasing variance as Bernstein's bound does. In the case where the variance is set constant and one increases the range R, apart from the worst-case scenario, Bernstein's bound becomes tighter as the condition $\sigma \ll R$ is approached.

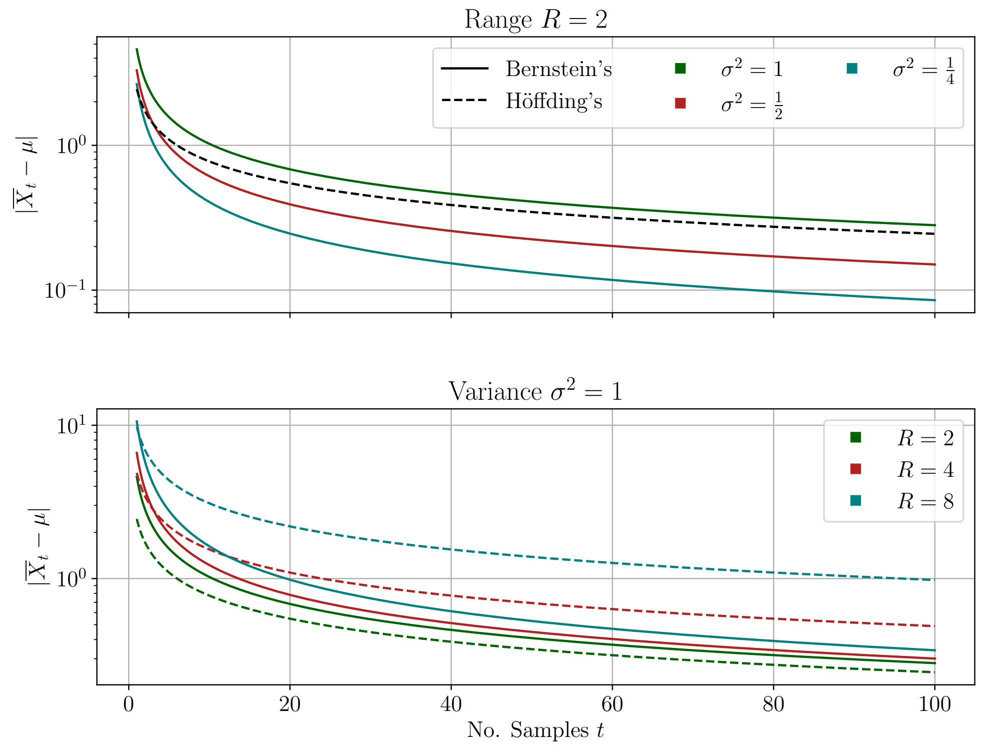

Figure 1: Bernstein's (20) and Höffding's bound (21) as a function of the number of samples t and the range R. Different values of R and σ are indicated by the corresponding colours respectively. Bernstein's bound is represented by a solid line, Höffding's with a dashed line. Further, the range is set to $R = 2$ in the top plot, while the variance is set to $\sigma^2 = R^2/4 = 1$ in the bottom figure. Note that in case of $R = 2$ and $\sigma^2 = 1$, Höffding's bound is tighter than Bernstein's, while for the other scenarios Bernstein's bound remain tighter for large t. The right-hand sides of the corresponding equations are plotted, see equations (20) & (21).

2.3. Quantum mechanics

This section gives a brief recap of quantum mechanics such as operators, Pauli matrices and two-level systems, while also briefly introducing the tensor product. With these concepts, quantum circuits and quantum gates are introduced. As a follow-up, variational quantum algorithms are introduced including the gradient-descent method to classically update the circuit's parameters.

2.3.1. Schrödinger's Equation

Quantum states can be represented using a state vector $|\psi\rangle$. This state vector contains all information of that particular system. Similar to Newton's second law, one can use Schrödinger's equation to calculate the time evolution of a given quantum state $|\psi\rangle$ based on a Hamiltonian $\hat{H}$. Schrödinger's equation is the fundamental equation in quantum mechanics and reads as follows:

$$i\hbar \frac{\partial |\psi(t)\rangle}{\partial t} = \hat{H} |\psi(t)\rangle . \tag{22}$$

The equation above is the time **time dependent** Schrödinger's equation. The **time independent** equation is as follows:

$$\hat{H}\left|\psi\right\rangle = E\left|\psi\right\rangle,$$

with E the energy of the state.
Solving the time in dependent Schrödinger's equation yields a state that is independent of time. To obtain a time evolution of such state, the unitary **time evolution operator** $\hat{U}(t - t_0)$ may be used. This operator propagates a state at a given time t_0 to a later time t.

$$\begin{aligned} \hat{U}(t, t_0) &= e^{-\frac{i\hat{H}}{\hbar}(t-t_0)} \\ \left|\psi(t)\right\rangle &= \hat{U}(t, t_0)\left|\psi(t_0)\right\rangle \\ &= e^{-\frac{i\hat{H}}{\hbar}(t-t_0)}\left|\psi(t_0)\right\rangle \end{aligned} \tag{23}$$

The state vector itself does not induce a probability density, only the modulus squared has physical meaning, as it is interpreted as a probability p_i:

$$p_i = |\langle i|\psi\rangle|^2. \tag{24}$$

2.3.2. Operators

An operator $\hat{A}$ is a linear function that maps a state $|\psi\rangle$, onto another state $|\phi\rangle$.

$$\hat{A}|\psi\rangle = |\phi\rangle, \tag{25}$$

if $|\psi\rangle \propto |\phi\rangle$ then $|\psi\rangle$ is a eigenstate of operator $\hat{A}$, i.e,:

$$\hat{A}|\psi\rangle = \lambda|\psi\rangle, \tag{26}$$

where λ the corresponding eigenvalue.
Two distinct eigenvectors of an operator are orthogonal to each other, if the operator is normalised. Concisely, with the Kronecker δ, this means that:

$$\langle\psi_i|\psi_j\rangle = \delta_{ij}. \tag{27}$$

In quantum mechanics, only eigenvalues are possible values for the outcomes of the corresponding observable $\hat{A}$. Any such operator that corresponds to an observable has to be linear and Hermitian, to ensures real eigenvalues.

$$\hat{A}(|f\rangle + |g\rangle) = (\hat{A}|f\rangle) + (\hat{A}|g\rangle) \qquad \text{(linear)} \tag{28}$$

$$\hat{A} = \hat{A}^\dagger \qquad \text{(Hermitian)} \tag{29}$$

Being linear, operators can also be expressed as matrices [2]:

$$\hat{A} = \begin{bmatrix} \langle\psi_1|\hat{A}|\psi_1\rangle & \dots & \langle\psi_1|\hat{A}|\psi_m\rangle \\ \langle\psi_2|\hat{A}|\psi_1\rangle & \dots & \langle\psi_2|\hat{A}|\psi_m\rangle \\ \vdots & \vdots & \vdots \\ \langle\psi_m|\hat{A}|\psi_1\rangle & \dots & \langle\psi_m|\hat{A}|\psi_m\rangle \end{bmatrix} = \begin{bmatrix} A_{11} & \dots & A_{1m} \\ A_{21} & \dots & A_{2m} \\ \vdots & \vdots & \vdots \\ A_{m1} & \dots & A_{mm} \end{bmatrix} \tag{30}$$

[2]This is only possible if the corresponding Hilbert-space is finite dimensional, e.g., when considering a finite number of basis states.

with $m < \infty$ and ψ_i, ψ_j being basis states.
Expressing operators as matrices will come in handy in later sections (see. sec. 2.4.3). The choice of the basis states is arbitrary. For instance, if $|\psi_i\rangle$ and $|\psi_j\rangle$ are chosen to be eigenstates of the operator A the corresponding matrix is diagonal.
The expectation value of operator $\hat{A}$ is given by:

$$\langle \hat{A} \rangle_\varphi = \langle \varphi | \hat{A} | \varphi \rangle . \tag{31}$$

Because expected values are always in relation to a particular state, we denote the state as a lower index as seen in equation (31). Using equation (6) the variance of an operator $\hat{A}$ can be calculated:

$$\mathrm{Var}(\hat{A}) = \langle \hat{A}^2 \rangle_\varphi - \langle \hat{A} \rangle_\varphi^2, \tag{32}$$

and the standard deviation:

$$\sigma = \sqrt{\mathrm{Var}(\hat{A})} = \sqrt{\langle \hat{A}^2 \rangle_\varphi - \langle \hat{A} \rangle_\varphi^2}. \tag{33}$$

2.3.3. Operator Exponential

Operators can also be convoluted by exponential functions. This is particularly handy for the time evolution operator $\mathrm{U}(t-t_0)$ (23). Take an operator $\hat{A}$ that can be expressed as an n×n matrix, then its operator exponential is defined as:

$$e^{\hat{A}} = \sum_{k=0}^{\infty} \frac{\hat{A}^k}{k!} = \mathbb{1} + \hat{A} + \frac{\hat{A}^2}{2!} + \frac{\hat{A}^3}{3!} + \dots \tag{34}$$

The notation $\hat{A}^n$ means that the operator $\hat{A}$ is applied n-times on a state $|*\rangle$:

$$\hat{A}^n |*\rangle = \underbrace{\hat{A}\hat{A}\dots\hat{A}}_{n\text{-times}} |*\rangle. \tag{35}$$

If, moreover, $A^2 = \mathbb{1}$, the matrix exponential $e^{i\theta A}$ can be calculated explicitly as can be neatly expressed as:

$$e^{i\theta\hat{A}} = \cos(\theta)\mathbb{1} + i\sin(\theta)\hat{A}. \tag{36}$$

A quick derivation of the equation (36) can be found in appendix (B).
Equation (36) can also be written as a matrix. For example set $\hat{A} = \sigma_X = X$ (see sec. 44):

$$e^{i\theta X} = \cos(\theta)\mathbb{1} + i\sin(\theta)X = \begin{bmatrix} \cos(\theta) & i\sin(\theta) \\ i\sin(\theta) & \cos(\theta) \end{bmatrix} \tag{37}$$

In this notation, the correspondence to a rotational matrix around the x-axis is apparent. This is why, we refer to eq. (36) as a rotational operator with rotation angle θ. We will revisit this in section 2.4.3.

2.4. Quantum computing

Quantum computing is computing using the phenomenons and principles of quantum mechanics. These properties are what makes quantum computing different from classical computing and where their potential lies in. For some problems, a quantum computer can have better time complexity, even to such extremes that they are only computable on them, in feasible time scales [18]. Achieving the later is known as **quantum advantage**. A practical quantum advantage has not been achieved yet, as the currently available quantum hardware is prone noise which limits their efficiency [19].

The fundamental information unit in quantum computing is the so-called qubit. Qubits are the quantum analogy to the classical bit. The aforementioned bit, can be either 0 or 1. A qubit, however, can be in the state $|0\rangle$ or $|1\rangle$ but also in any superposition of these two. These qubits can be transformed by unitary gates, some of which coincide with operators from a quantum mechanics text book such as the Pauli matrices. Quantum circuits essentially are a sequence of these gates, similar to a classical circuit.
The following section introduces qubits, prominent gates and a short exemplary circuit. Lastly, VQAs are introduced as well as their classical optimization loop.

2.4.1. Qubits

Qubits are two-state systems that form the fundamental information units in quantum computing, similarly to the bit in classical computing. Since a qubit can exist in a superposition of its two basis states, $|0\rangle$ and $|1\rangle$, we can express an arbitrary single-qubit state as:

$$|\psi\rangle = \alpha|0\rangle + \beta|1\rangle = \begin{bmatrix}\alpha \\ \beta\end{bmatrix}, \tag{38}$$

with $\alpha, \beta \in \mathbb{C}$ and $|\alpha|^2 + |\beta^2| = 1$.
The $|0\rangle$ and $|1\rangle$ states have already been introduced as the eigenvectors of the σ_z Pauli matrix, see section 44. Since choosing a basis is arbitrary, the convention is to refer to these basis states as the computational basis states. Sometimes it is illustrative to express the complex coefficients α and β to a different form [19]. Using $|\alpha|^2 + |\beta|^2 = 1$ and the Pythagorean trigonometric identity, we can write the equation in terms of the angles φ and θ:

$$|\psi\rangle = \cos\left(\frac{\theta}{2}\right)|0\rangle + e^{i\varphi}\sin\left(\frac{\theta}{2}\right)|1\rangle, \tag{39}$$

with $\varphi, \theta \in \mathbb{R}$.
By virtue of equation (39), all possible qubit states can be represented on a so-called Bloch sphere, see figure 2. Every point on this Bloch sphere is a valid qubit (pure) state, defined up to a global phase, thus giving infinite possibilities for a state representation. A mixed state [3] is represented on the Bloch sphere by a state within it [19].

[3] Pure states are states that can be represented by a density matrix, i.e., $\rho = |\psi\rangle\langle\psi|$. Mixed states are represented by a convex sum, i.e., $\rho_{\text{mixed}} = \sum_i \alpha_i |\psi_i\rangle\langle\psi_i|$.

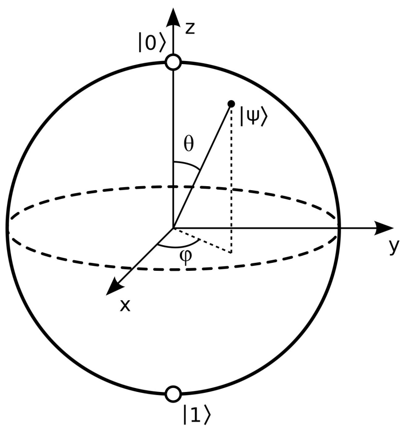

Figure 2: Bloch sphere [20]. Each axis corresponds to a pair of Pauli vectors (45). For example, the poles of the z-axis correspond to $|0\rangle$ and $|1\rangle$, respectively. The angle $\theta \in [0, \pi]$ is relative to the z-axis and the angle $\varphi \in [0, 2\pi)$ is relative to the x-axis. Any point on and inside this sphere represents a valid state.

Multi-qubit states

For any meaningful quantum computation, a single qubit is not sufficient. Bigger qubit systems are necessary to facilitate complex quantum computations. An n-qubit quantum system is simply created by combining n individual qubits together. The corresponding mathematical operation that is used for combining such physical systems is the tensor product , e.g.:

$$|0\rangle^{\otimes n} = |0\rangle_1 \otimes |0\rangle_2 \otimes \ldots \otimes |0\rangle_n = |\underbrace{0\ldots0}_{\mathrm{n}}\rangle. \tag{40}$$

For $n = 2$ this is called a two qubit system. Such two qubit systems have four computational basis states:

$$|00\rangle = \begin{bmatrix}1\\0\\0\\0\end{bmatrix}, \quad |01\rangle = \begin{bmatrix}0\\1\\0\\0\end{bmatrix}, \quad |10\rangle = \begin{bmatrix}0\\0\\1\\0\end{bmatrix}, \quad |11\rangle = \begin{bmatrix}0\\0\\0\\1\end{bmatrix}. \tag{41}$$

Any two-qubit state may be in a superposition of these four basis:

$$|\psi\rangle = \alpha\,|00\rangle + \beta\,|01\rangle + \gamma\,|10\rangle + \delta\,|11\rangle. \tag{42}$$

This state also must fulfil the normalisation condition for it to be a physically acceptable state:

$$|\alpha|^2 + |\beta|^2 + |\gamma|^2 + |\delta|^2 = 1. \tag{43}$$

This can be extended to an n qubit system analogously.
As qubits are two-state systems, similarly to spin systems, $|0\rangle$ and $|1\rangle$ are Pauli eigenvectors. In the next section, the eigenvectors and values of the three Pauli matrices are introduced, as they play a fundamental role in quantum computing.

2.4.2. Pauli Operators/ Matrices

Pauli matrices play an import role not only in spin physics but also in quantum computation. These matrices are Hermitian and unitary[4] and given as:

$$X = \sigma_x = \begin{bmatrix} 0 & 1 \\ 1 & 0 \end{bmatrix}, \qquad Y = \sigma_y = \begin{bmatrix} 0 & -i \\ i & 0 \end{bmatrix}, \qquad Z = \sigma_z = \begin{bmatrix} 1 & 0 \\ 0 & -1 \end{bmatrix}. \tag{44}$$

Note that the Pauli matrices, together with the identity span a basis for every complex 2×2 matrix. They all share the same two eigenvalues, $+1$ and -1. Their corresponding eigenvectors are:

$$|+\rangle = |x_+\rangle = \frac{1}{\sqrt{2}} \begin{bmatrix} 1 \\ 1 \end{bmatrix}, \qquad |-\rangle = |x_-\rangle = \frac{1}{\sqrt{2}} \begin{bmatrix} 1 \\ -1 \end{bmatrix}, \tag{45}$$

$$|i\rangle = |y_+\rangle = \frac{1}{\sqrt{2}} \begin{bmatrix} 1 \\ i \end{bmatrix}, \qquad |-i\rangle = |y_-\rangle = \frac{1}{\sqrt{2}} \begin{bmatrix} 1 \\ -i \end{bmatrix}, \tag{46}$$

$$|0\rangle = |z_+\rangle = \begin{bmatrix} 1 \\ 0 \end{bmatrix}, \qquad |1\rangle = |z_-\rangle = \begin{bmatrix} 0 \\ 1 \end{bmatrix}. \tag{47}$$

Note that the convention in the context of quantum computing is to refer to σ_x, σ_y and σ_z as X, Y and Y respectively. Correspondingly, the eigenvectors are denoted differently as well. None of these matrices commute with each other. This can be condensely expressed with a single commutation equation[5]:

$$[\sigma_a, \sigma_b] = 2i\varepsilon_{abc}\sigma_c. \tag{48}$$

A useful way to write the Pauli matrices is to write them in terms of in terms of the computational basis, using the Dirac notation.

$$\sigma_x = |1\rangle\langle 0| + |0\rangle\langle 1|, \quad \sigma_y = i|1\rangle\langle 0| - i|0\rangle\langle 1|, \quad \sigma_z = |0\rangle\langle 0| - |1\rangle\langle 1|. \tag{49}$$

2.4.3. Quantum Gates

Quantum gates are unitary operators that map qubit states to qubit states. They are the elementary operations of a quantum circuit. One important difference from classical gates is the fact that quantum gates have to be reversible since the gates are unitary and thus reversible. [19].

A quantum circuit consisting of a sequences of quantum gates can be visualised by a circuit diagram. In these diagrams time flows from left to right and multiple qubits are stacked vertically. The order in which the operators operate is, thus, also determined by this direction. For example, take one arbitrary single qubit gate and a single-qubit gate A, a circuit could look like:

$$|\alpha\rangle \;—\boxed{A}—\; |\beta\rangle$$

While gates are, in principle, not limited in the number of qubits they act on, most only act on on one or two qubits. This is because every n-qubit unitary can arbitrarily well-approximated by a sequence of single- and two-qubit gates single- or two-qubit gate [19]. Moreover, there exist finite sets of quantum gates, called universal gate sets, with which it is possible to represent any

[4]A matrix A is called unitary if and only if: $A^\dagger A = AA^\dagger = \mathbb{1}$.

[5]with ϵ_{abc} being the Levi-Civita symbol and using the Einstein summation convention

unitary operation up to any arbitrary precision [21]. Hence, such a universal gate set is, in principle, sufficient for all computations.
Various prominent examples of single- and two-qubit gates are introduced in the following.

Identity Gate

A trivial example for a gate is the **identity gate**. Mathematically, it is the identity matrix $\mathbb{1}_{2x2}$ and does not alter the state on which it acts. For a single qubit:

$$\mathbb{1} = \begin{bmatrix} 1 & 0 \\ 0 & 1 \end{bmatrix} = |0\rangle\langle 0| + |1\rangle\langle 1|. \tag{50}$$

Pauli Gates

The Pauli matrices also can be used as gates because they are unitary as well. All three of them rotate a given state along the corresponding axis by π on the Bloch sphere.

X-gate / NOT-gate

The X-gate is also called the **bit-flip** gate because it maps $|0\rangle$ to $|1\rangle$ and $|1\rangle$ to $|0\rangle$. It is equivalent to the NOT gate from classical circuits [22].
X acts on $|0\rangle$ and $|1\rangle$ as follows:

$$X|0\rangle = (|1\rangle\langle 0| + |0\rangle\langle 1|)|0\rangle = |1\rangle, \tag{51}$$
$$X|1\rangle = (|1\rangle\langle 0| + |0\rangle\langle 1|)|1\rangle = |0\rangle. \tag{52}$$

Y-gate

The Y-gate interchanges $|0\rangle$ and $|1\rangle$ like the X-gate with the exception of an additional phase.
Y-gate acts on $|0\rangle$ and $|1\rangle$ as follows:

$$Y|0\rangle = (i|1\rangle\langle 0| - i|0\rangle\langle 1|)|0\rangle = +i|1\rangle, \tag{53}$$
$$Y|1\rangle = (i|1\rangle\langle 0| - i|0\rangle\langle 1|)|1\rangle = -i|0\rangle. \tag{54}$$

Z-gate

The Z-gate is also called the **phase flip** as it introduces a relative phase between the computational basis states
Z-gate acts on $|0\rangle$ and $|1\rangle$ as follows:

$$Z|0\rangle = (|0\rangle\langle 0| - |1\rangle\langle 1|)|0\rangle = +|0\rangle, \tag{55}$$
$$Z|1\rangle = (|0\rangle\langle 0| - |1\rangle\langle 1|)|1\rangle = -|1\rangle. \tag{56}$$

Rotation Gates

The previous Pauli gates can only rotate a state by a fixed angle of π their respective axis. To rotate a state by an arbitrary angle θ along an axis, the **Pauli rotation** gates [22] may be used. These gates are generated by the Pauli operators as the exponential as in equation (36).

R_X-gate

The R_X-gate rotates a state along the x-axis by θ. Using equation (36):

$$R_X(\theta) := e^{-i\frac{1}{2}\theta X} = \cos\left(\frac{\theta}{2}\right)\mathbb{1} - i\sin\left(\frac{\theta}{2}\right)X = \begin{bmatrix} \cos\left(\frac{\theta}{2}\right) & -i\sin\left(\frac{\theta}{2}\right) \\ -i\sin\left(\frac{\theta}{2}\right) & \cos\left(\frac{\theta}{2}\right) \end{bmatrix}$$

In particular, setting $\theta = \pi$ yields the X-gate up to a global phase $-i$:

$$R_X(\pi) := e^{i\frac{\pi}{2}}X = \begin{bmatrix} 0 & -i \\ -i & 0 \end{bmatrix} = -iX. \tag{57}$$

R_Y-gate

Analogously, the R_Y-gate rotates a state along the y-axis by θ.

$$R_Y(\theta) := e^{-i\frac{1}{2}\theta Y} = \cos\left(\frac{\theta}{2}\right)\mathbb{1} - i\sin\left(\frac{\theta}{2}\right)Y = \begin{bmatrix} \cos\left(\frac{\theta}{2}\right) & -\sin\left(\frac{\theta}{2}\right) \\ \sin\left(\frac{\theta}{2}\right) & \cos\left(\frac{\theta}{2}\right) \end{bmatrix}$$

R_Z-gate

The R_Z-gate rotates a given state along the z-axis by θ:

$$R_Z(\theta) := e^{-i\frac{1}{2}\theta Z} = \cos\left(\frac{\theta}{2}\right)\mathbb{1} - i\sin\left(\frac{\theta}{2}\right)Z = \begin{bmatrix} e^{-i\frac{\theta}{2}} & 0 \\ 0 & e^{i\frac{\theta}{2}} \end{bmatrix} \tag{58}$$

When multiple rotations are performed, they can be combined into to a single gate using the **Baker–Campbell–Hausdorff formula** [19]. Which provides a closed-form solution to the equation $e^A e^B = e^C$, with A, B and C operators with:

$$C = A + B + \frac{1}{2}[A, B] + \frac{1}{12}[A, [A, B]] - \frac{1}{12}[B, [A, B]] + \cdots \tag{59}$$

When two rotations are performed along the same axis, for example the X-axis, the angles are simply added up. Verifying this is straight forward due to the commutation relation for the X Pauli operator (see eq. (48)), i.e. $[X, X] = 0$:

$$R_X(\theta)R_X(\varphi)|*\rangle = \left(e^{-i\frac{\theta}{2}X} e^{-i\frac{\varphi}{2}X}\right)|*\rangle = e^{-i\frac{\theta+\varphi}{2}X}|*\rangle = R_X(\theta+\varphi)|*\rangle, \tag{60}$$

with $|*\rangle$ being an arbitrary single qubit state.
The circuit diagram consequently is as follows:

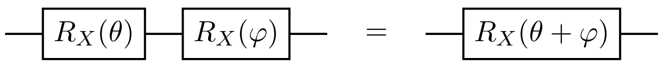

Hadamard gate

The so-called Hadamard gate H, creates an equal superposition of the computational basis states.

$$H = \frac{1}{\sqrt{2}}\begin{bmatrix} 1 & 1 \\ 1 & -1 \end{bmatrix} = \frac{1}{\sqrt{2}}\left(|0\rangle\langle 0| + |0\rangle\langle 1| + |1\rangle\langle 0| - |1\rangle\langle 1|\right). \tag{61}$$

In fact, this gate maps the $|0\rangle$ to the $|+\rangle$ state and the $|1\rangle$ to the $|-\rangle$. The states $|+\rangle$ and $|-\rangle$ are introduced in section 2.4.2. Therefore, the Hadamard directly maps the computational basis to the Pauli Y-basis (sometimes also called the Hadamard basis).

$$H|0\rangle = \frac{1}{\sqrt{2}}\begin{bmatrix}1 & 1\\ 1 & -1\end{bmatrix}|0\rangle = \frac{1}{\sqrt{2}}|0\rangle + \frac{1}{\sqrt{2}}|1\rangle = |+\rangle \tag{62}$$

$$H|1\rangle = \frac{1}{\sqrt{2}}\begin{bmatrix}1 & 1\\ 1 & -1\end{bmatrix}|1\rangle = \frac{1}{\sqrt{2}}|0\rangle - \frac{1}{\sqrt{2}}|1\rangle = |-\rangle. \tag{63}$$

Lastly, applying the H-gate twice will not alter the state. Because $HH = \mathbb{1}_{2\times 2}$.

$$H(H|0\rangle) = H|+\rangle = |0\rangle, \tag{64}$$

$$H(H|1\rangle) = H|-\rangle = |1\rangle. \tag{65}$$

CNOT-gate

In contrast to the other gates in this section, the CNOT-gate takes two qubits as its input. The first qubit acts as the control qubit, the other as the target. As the name suggest, the control qubit dictates how the target qubit is altered. The control qubit remains unaffected and the X-gate is applied to the target qubit if and only if the control qubit is in the $|1\rangle$ state.

$$\text{CNOT} = \begin{bmatrix}1 & 0 & 0 & 0\\ 0 & 1 & 0 & 0\\ 0 & 0 & 0 & 1\\ 0 & 0 & 1 & 0\end{bmatrix} \tag{66}$$

For example, if the CNOT-gate acts on the state $|11\rangle$:

$$\begin{aligned}\text{CNOT}|11\rangle &= \begin{bmatrix}1 & 0 & 0 & 0\\ 0 & 1 & 0 & 0\\ 0 & 0 & 0 & 1\\ 0 & 0 & 1 & 0\end{bmatrix}\begin{bmatrix}0\\0\\0\\1\end{bmatrix} = \begin{bmatrix}0\\0\\1\\0\end{bmatrix}\\ &= |1\rangle \otimes X|1\rangle = |1\rangle \otimes |0\rangle = |10\rangle\end{aligned} \tag{67}$$

The full effect of the CNOT-gate is listed inin table 1. Lastly, this controlled two-qubit gate operation can be generalised to the controlled-U gate:

$$CU = \begin{bmatrix}1 & 0 & 0 & 0\\ 0 & 1 & 0 & 0\\ 0 & 0 & U_{00} & U_{01}\\ 0 & 0 & U_{10} & U_{11}\end{bmatrix} \tag{68}$$

This gate applies the unitary U in the same manner as the CNOT-gate applies the X-gate. A tabular summary of the previously introduced gates can be seen in appendix B.

Table 1: Truth table of the CNOT-gate for the computational basis states.

Before	After
$\|00\rangle$	$\|00\rangle$
$\|01\rangle$	$\|01\rangle$
$\|10\rangle$	$\|11\rangle$
$\|11\rangle$	$\|10\rangle$

2.4.4. Measurements in Different Bases

Measurements are performed in the computational basis, which - by convention - coincides with the Pauli-z basis, by default. In a circuit diagram this is represented by the according measurement symbol. For example:

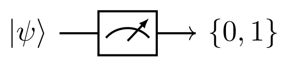

By the postulates of quantum mechanics, such a measurement collapses the quantum state to one of the computational basis states and produces one bit of classical information, according to the collapsed state. Therefore, before performing the measurements again, requires the re-preparation of that state. Measurements result in either the 0 or 1 bit, depending on the measured state. If an n-qubit system is measured like this qubit-by-qubit, a bit-string, $\{0,1\}^n$, is produced. However, a different basis measurement can also be selected. Of particular interest are the three Pauli bases, see Bloch sphere 2. In order to measure in either the Pauli X or Y basis in similar fashion, the state has to be transformed first.
Solving this problem is a basic one in linear algebra as it essentially boils down to a basis transformation. For example, the Hadamard gate H maps the states $|0\rangle$ and $|1\rangle$ following eq. (62) & (63). Applying the Hadamard gate the other way around results in the wanted transformation:

$$|+\rangle \mapsto |0\rangle \tag{69}$$

$$|-\rangle \mapsto |1\rangle \, . \tag{70}$$

After this operation, the state $|0\rangle$ is measured if and only if the quantum state has previously been the $|+\rangle$-state. As a consequence, measuring this state will yield the standard bit-string $\{0,1\}$ as desired.
The measurement in the Pauli Y-basis can also be achieved with an additional phase gate S Hence, applying the right unitary transformation before measuring allows for measurements in different bases. These unitaries are listed in table 2.

Table 2: Unitary transformation for measurement in different bases.

Basis	Unitary
Z	$-\boxed{\mathbb{1}}-$
X	$-\boxed{S^\dagger}-\boxed{H}-$
Y	$-\boxed{H}-$

with $S^\dagger = (H\sqrt{X}H)^\dagger$.

2.4.5. Variational Quantum Algorithms

Variational quantum algorithms (VQA) are one of many methods that aim to utilise the currently available quantum hardware with all of its limitations. These limitations range from the limited qubit number to the limited circuit depths and general noise concerns [4, 19]. VQAs approach these limitations by using an optimization-based method. The idea is to outsource the optimization to classical computers, which interface with the quantum computer by parameters of a parameterised quantum circuit.
VQAs may lead to a general quantum advantage on currently available NISQ hardware. The proposed use-cases for VQAs are in quantum chemistry, e.g., finding ground states, combinatorial problems, or linear algebra problems, i.e. solving large systems of linear equations [4]. A simple schematic overview of a VQA can be see in figure 3.

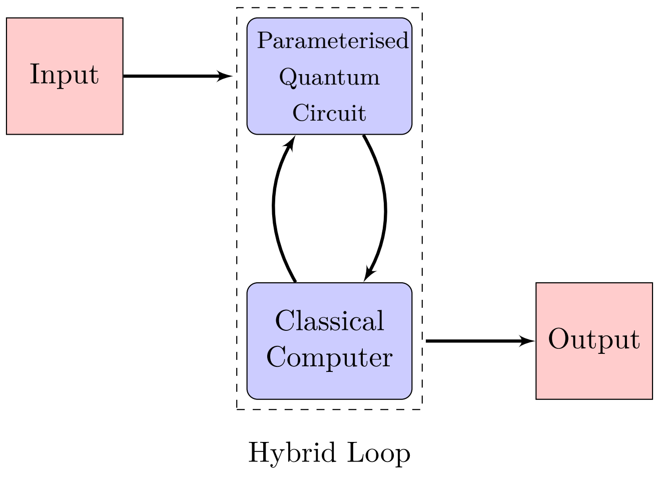

Figure 3: Simple schematic of a variational quantum algorithm (VQA). The inputs of a VQA are the Hamiltonian providing the cost function and the ansatz (the layout of the parameterised circuit). The quantum circuit prepares a quantum state to be measured repeatedly and the classical computer in return calculates the next set of parameters based on the chosen optimisation routine. The desired output in our case should correspond to the set of parameters that minimises the cost function, e.g., the ground-state of the Hamiltonian.

In order to define the problem instance for the VQA, a so called cost function C has to be defined. The purpose of the VQA is to minimize this cost function by finding a set of parameters $\boldsymbol{\theta}$ that minimizes, i.e., to ideally find .

$$\boldsymbol{\theta}_{\min} = \arg\min_{\boldsymbol{\theta}} C(\boldsymbol{\theta}). \tag{71}$$

The cost function together with the parameter space makes up the **cost landscape**. Its dimension equals the number of parameters. A cost function, for example, could be the expectation value of the given Hamiltonian or a spin measurement. In this case, the landscape is a energy landscape. Finding a global or local minimum in this energy landscape, essentially is the task of the VQA. The cost function in this case has the form [4]:

$$C(\boldsymbol{\theta}) = \langle \psi_0 | \hat{U}^\dagger(\boldsymbol{\theta}) \hat{O} \hat{U}(\boldsymbol{\theta}) | \psi_0 \rangle. \tag{72}$$

with ψ_0 being the initial input state for the circuit, $\hat{O}$ the observable (e.g. Hamiltonian), $\hat{U}(\boldsymbol{\theta})$ a parameterised unitary, i.e., the parameterised circuit. The parameterised circuit is typically represented by multiple layers of unitaries $\hat{U}_i(\theta_i)$ that multiply up to the whole circuit $\hat{U}(\boldsymbol{\theta})$ as seen in Figure 4. Such unitary $\hat{U}(\boldsymbol{\theta})$ can be expressed as:

$$\hat{U}(\boldsymbol{\theta}) = \hat{U}(\theta_1) \cdot \hat{U}(\theta_2) \cdot \ldots \cdot \hat{U}(\theta_L). \tag{73}$$

The explicit form of each layer depends on the ansatz made. An initial state $|\psi_0\rangle$ with a given ansatz $\hat{U}(\boldsymbol{\theta})$, i.e. the circuit, results in the parameterised state $|\psi(\boldsymbol{\theta})\rangle$.

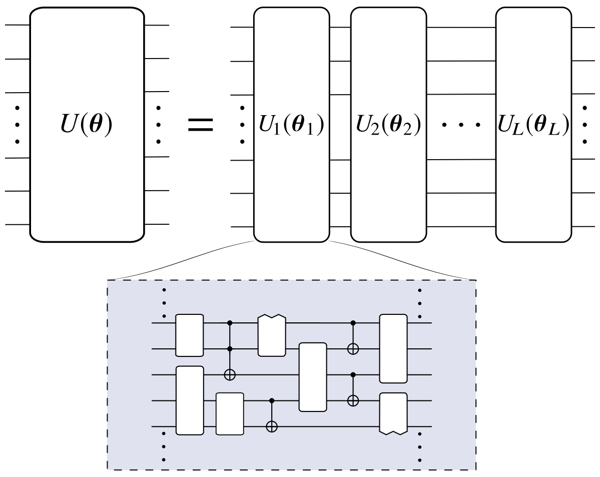

$U(\boldsymbol{\theta})$
=
$U_1(\boldsymbol{\theta}_1)$
$U_2(\boldsymbol{\theta}_2)$
$\cdots$
$U_L(\boldsymbol{\theta}_L)$

Figure 4: Parameterised circuit example circuit with L layers of unitaries. Each layer $\hat{U}_i(\theta_i)$ depends only on a single parameter θ_i. Stacking up these layers results in the unitary $\hat{U}(\boldsymbol{\theta})$. The blue box shows an example circuit for a single layer which can at most depend on θ_i. Figure taken from [4].

The classical computer then evaluates the value of the cost function from repeated measurements and applies a classical optimisation method. The task of the classical computers is to choose the next set of parameters $\boldsymbol{\theta}$ to navigate downwards in the cost landscape. Subsequently, the **hybrid loop** repeats. How the navigation is done depends on the method used for the optimization routine. The most commonly used is the so-called **gradient descent method**. Although there are more available methods, in this thesis, the gradient descent method is the method of choice.

Gradient Descent

The gradient-descent method updates a set of parameters $\boldsymbol{\theta}$ by using the gradient of the cost function with respect to $\boldsymbol{\theta}$ such that the updated direction points to the direction in the cost landscape where the slope is the steepest. This is done by setting a learning rate α and calculating the gradient at the current point $\boldsymbol{\theta}_k$.

$$\boldsymbol{\theta}_{k+1} = \boldsymbol{\theta}_k - \alpha \nabla C(\boldsymbol{\theta}_k). \tag{74}$$

Using equation (74), a classical computer calculates the next set of parameters to navigate in the cost landscape. By doing so, (local) minima can be reached.

However, calculating the gradient of the cost function is not always analytically possible and one has to settle for approximative methods for the gradient estimation. A method of calculating quantum gradients is the so called **simultaneous perturbation stochastic approximation** (SPSA) introduced in Ref. [23]. SPSA requires two circuit calls per gradient estimation, whereas the parameter shift rule scales linearly with the number of circuit parameters, making it advantageous for large circuits because of the constant scaling. The SPSA method achieves this by estimating the cost function at $\boldsymbol{\theta} + \mu\Delta$ and $\boldsymbol{\theta} - \mu\Delta$, where an element of Δ, Δ_i is defined as:

$$\Delta_i = \begin{cases} +1 & \text{with probability } 50\% \\ -1 & \text{otherwise} \end{cases} \tag{75}$$

with $i = \{1, \dots, N\}$, N being the number of parameters and $\mu \in \mathbb{R}$ a small parameter.
The gradient is calculated by the following equation:

$$\nabla C(\boldsymbol{\theta}) \approx \frac{C(\boldsymbol{\theta} + \mu\Delta) - C(\boldsymbol{\theta} - \mu\Delta)}{2\mu\Delta}. \tag{76}$$

This method provides faster gradient estimations and improved accuracy, compared to the parameter shift rule, see ref. [23] and appendix B.2. Especially for higher numbers of parameters, due to the constant scaling of the SPSA method, compared to the $2n$ (n is the number of qubits) scaling of other conventional methods.
For example, the gradient descent method on a one-dimensional energy landscape, thus having only one parameter θ, can be seen in figure 5.

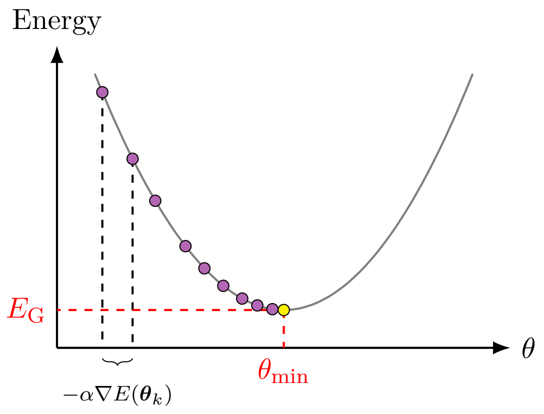

Figure 5: Gradient descent on a one-dimensional energy landscape. The yellow dot is at $\boldsymbol{\theta}_{\mathrm{min}}$ and bears the ground energy E_{G} of this energy landscape. On every purple dot, a measurement of the energy $E(\boldsymbol{\theta}_k)$ has been made. The next parameter $\boldsymbol{\theta}_{k+1}$ is calculated based on the measured gradient $\nabla E(\boldsymbol{\theta}_k)$ from the previous step. By walking stepwise through the landscape, with the right learning rate α, eventually an energy $E(\boldsymbol{\theta}_k) \approx E_{\mathrm{G}}$ (yellow dot) will be reached. In the region near an extremum or saddle point, that is, where the gradient is small, the number of steps to advance further becomes larger. This is shown by the purple dots being closer to each other near the yellow dot.

Variational Quantum Eigensolvers

The most variant of VQAs is the so-called **variational quantum eigensolver** (VQE). It is used to estimate ground-state eigenvalues and eigenstates of a given Hamiltonian $\hat{H}$ [4]. In this case, the cost function (see eq. (72)) is given by the expectation value of $\hat{H}$ with a parameterised state $|\psi(\boldsymbol{\theta})\rangle$:

$$C(\boldsymbol{\theta}) = \langle\psi(\boldsymbol{\theta})|\hat{H}|\psi(\boldsymbol{\theta})\rangle \coloneqq E(\boldsymbol{\theta}). \tag{77}$$

with $E(\boldsymbol{\theta})$ being the energy depending on the parameters $\boldsymbol{\theta}$. From now on, the cost function will be called $E(\boldsymbol{\theta})$. Using the Rayleigh-Ritz variational method the energy $E(\boldsymbol{\theta})$ is lower bounded by the ground state energy, i.e.

$$E_{\mathrm{G}} \leq E(\boldsymbol{\theta}). \tag{78}$$

The Hamiltonian for a VQE is usually decomposed as a sum of multi-qubit Pauli operators $\sigma_i^{(k)}$ [6] (see sec. 2.4.2):

$$\hat{H} = \sum_i c_i P_i, \tag{79}$$

with $c_i \in \mathbb{R}$ and $P_i \in \{X, Y, Z, \mathbb{1}\}^{\otimes n}$.
It is common to represent a Hamiltonian as a sum of Pauli operators, as these are easily implementable. The typical procedure for a VQE can be seen in figure 6.

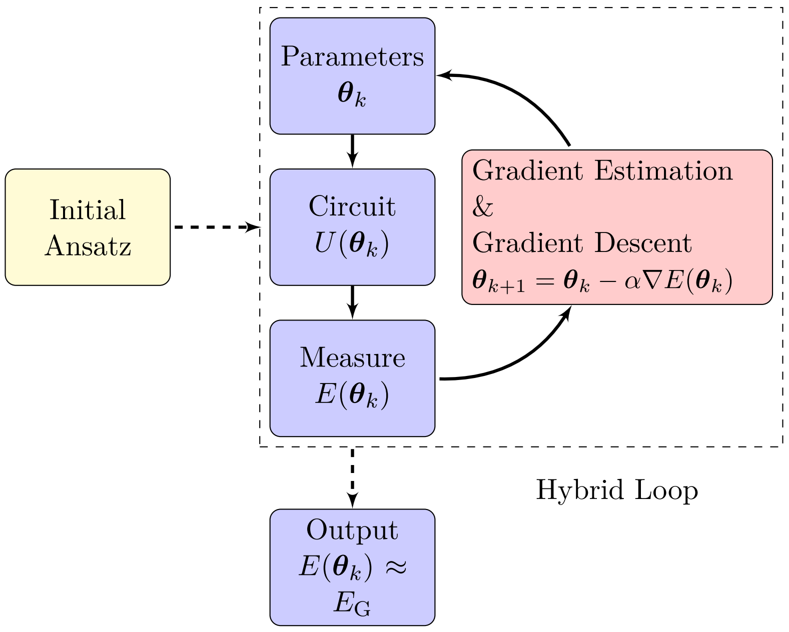
Parameters $\boldsymbol{\theta}_k$
Initial Ansatz
Circuit $U(\boldsymbol{\theta}_k)$
Gradient Estimation & Gradient Descent $\boldsymbol{\theta}_{k+1} = \boldsymbol{\theta}_k - \alpha\nabla E(\boldsymbol{\theta}_k)$
Measure $E(\boldsymbol{\theta}_k)$
Hybrid Loop
Output $E(\boldsymbol{\theta}_k) \approx E_{\mathrm{G}}$

Figure 6: Flow chart of a VQE. The circuit layout is set by the Ansatz, shown in yellow. The dashed box corresponds to the hybrid loop in which the quantum circuit and the classical optimizer work together. In each loop, the circuit provides the classical optimizer the current energy $E(\boldsymbol{\theta}_k)$ from which it calculates the next set of parameters $\boldsymbol{\theta}_{k+1}$. At that point, the loop continues with $\boldsymbol{\theta}_{k+1}$ as the new starting parameters. The loop is based on figure 3.

[6] This operator acts on the k-th qubit.

3. Methods

This section provides an introduction to the empirical Bernstein stopping algorithm (EBS) and the layout of the VQE (see sec. 2.4.5) used as a benchmark. To that extend, first EBS itself and some modifications are introduced. These modified algorithms are then compared against each other and also to the Höffding's bound (see eq. (15)). Secondly, we explain how to set-up a VQE as a benchmarking tool for EBS. This includes, in particular, the quantum decomposition that yields a circuit representation for a unitary operator. Lastly, we illustrate on how to interconnect EBS with the hybrid loop of an VQE

3.1. Empirical Bernstein Stopping (EBS)

Sampling is a resource intensive task in quantum computing or machine learning. In the case of quantum computing, the result of a computation has to be read-off via a measurement. However, due to the fundamental nature of quantum mechanics, any measurement projects the state into a single outcome with a certain probability. Therefore, this process has to be repeated to achieve an accurate result.
The naive approach arguably is to fix a number of samples that can be taken for each estimate, this approach does not provide any guarantees for the produced estimate. It would be beneficial to have algorithms, that For this purpose there are algorithms, which control the sampling process based on set parameters and terminate when a fixed accuracy is reached. One such algorithm is the **empirical Bernstein stopping algorithm** (EBS) developed by Mnih *et al.* [16]. EBS is an adaptive stopping algorithm as it immediately processes the samples that are drawn. In particular, it calculates the running empirical variances. By employing the empirical Bernstein inequality, eq. (19), this allows EBS to be used in cases where the variance of the underlying probability distribution is not known, i.e., most practical scenarios.
In the following section, first the concept of a (ϵ, δ)-stopping rule is introduced followed by the base EBS algorithm, in both a relative error and absolute error version. Secondly, an improvement to the base EBS algorithm is discussed and compared to the base version. Lastly a comparison to a non-adaptive sample algorithm like Höffding's bound is made.

3.1.1. (ϵ, δ)-Stopping Rules

A stopping rule $\mathbf{S}$ is a condition that when met will terminate an algorithm. In addition, we require a stopping rule to terminate the algorithm eventually. Mathematically, this can be expressed as:

$$\mathbb{E}[T(\mathbf{S})] < \infty \tag{80}$$

with $T(\mathbf{S})$ being the time the stopping algorithm terminates.
This condition formally requires that the algorithm terminates in a finite amount of time. There are many ways ways to do so. However, but the focus in this thesis is on stopping rules that are constructed from concentration inequalities. These are the so-called (ϵ, δ)-stopping rules.
An (ϵ, δ) stopping rule takes two parameters, δ the maximal tolerated probability of failure ($1 - \delta$ is often called confidence) and ϵ the relative accuracy

that the returned estimate should should at least have. Any stopping rule **S** that satisfies the following condition is an (ϵ, δ)-stopping rule [16]:

$$\mathbb{P}[|\hat{\mu} - \mu| \leq \epsilon|\mu|] \geq 1 - \delta \tag{81}$$

with $\hat{\mu}$ the estimated expected value of a real-valued random variable given as the return value of an algorithm and μ being the expected value. Any stopping rule **S** that fulfils equation (81) ensures, with probability of at least $1 - \delta$ that when it terminates the estimated expected value $\hat{\mu}$ will only be within a relative error ϵ of the expected value μ:

$$|\hat{\mu} - \mu| \leq \epsilon|\mu| \tag{82}$$

If one considers an absolute error, one simply considers following instead:

$$\mathbb{P}[|\hat{\mu} - \mu| \leq \epsilon] \geq 1 - \delta, \tag{83}$$

$$|\hat{\mu} - \mu| \leq \epsilon. \tag{84}$$

Henceforth, if not stated otherwise, accuracies in this thesis are considered absolute.

3.1.2. Empirical Bernstein Stopping Rule

In the following, we demonstrate that the Bernstein inequality can be used to create an (ϵ, δ) stopping rule. The detailed derivation can be found in on Ref. [16].
Let $\mathcal{F}$ be the event in which the stopping rule fails, i.e., the algorithm stops but the required accuracy is not met.

$$\mathcal{F} = \{|\hat{\mu} - \mu| \geq \epsilon\} \tag{85}$$

Further, define T_{failure} be the time for $\mathcal{F}$.
As Bernstein's inequality (17), assumes the full failure provability δ at every step t, the probability for the event $\mathcal{F}$ can be calculated by summing up all time steps:

$$\mathbb{P}[\mathcal{F}] = \sum_{t=1}^{\infty} \mathbb{P}[\mathcal{F} \cap \{t = T_{\text{failure}}\} \overset{!}{\leq} \delta \tag{86}$$

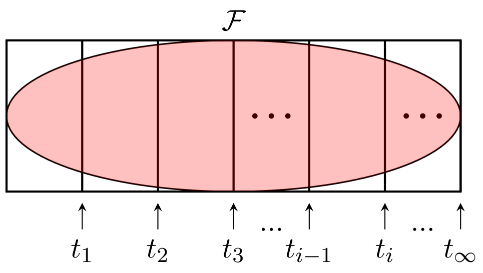

Figure 7: A more approachable representation of equation (86). $\mathcal{F}$ is represented by the red elliptical set and the areas created by vertical lines represent disjoint subsets where $t_i = T_{\text{Failure}}$. The total probability of $\mathcal{F}$ are all the times t_i the algorithm terminates but fails to deliver a return $\hat{\mu}$ that is within ϵ of the expected value μ, i.e., the sum of the measures of all the subsets.

The idea is to define a sequence of partial failure probability $\{d_t\}$. An element d_t of this sequence can be understood as the partial failure probability for the segments in figure 7. Hence, following inequality holds:

$$\mathbb{P}[\mathcal{F} \cap \{t = T_{\text{failure}}\}] \leq d_t. \tag{87}$$

Following equation 86, the sequence $\{d_t\}$ must fulfil:

$$\sum_{t=1}^{\infty} d_t \leq \delta \tag{88}$$

The author recommends following choice of d_t:

$$d_t = \frac{c}{t^p}, \tag{89}$$

with $c = {}^{\delta(p-1)}/{}_{p}$ and $p > 1$ as the optimal choice. Further discussion of this choice can be found in Ref. [16].
The empirical Bernstein bound holds for every time t (17), which serves as a useful lower-bound for each d_t:

$$\mathbb{P}[|\overline{X}_t - \mu| \geq \epsilon] \leq 2\exp\left(-\frac{(t\epsilon)^2/2}{\sigma_t^2 + Rt\epsilon/3}\right) \leq d_t \tag{90}$$

This equation can be rewritten into a bound form similar to equation (18):

$$|\overline{X}_t - \mu| \leq \epsilon \leq \sqrt{\frac{2\overline{V}_t \ln\left(\frac{3}{d_t}\right)}{t}} + \frac{2R\ln\left(\frac{3}{d_t}\right)}{t} := c_t \tag{91}$$

This equation holds with probability of at least $1 - d_t$.
Compared to the empirical Bernstein bound, see eq. (19), eq. 91 assumes a partial failure probability d_t instead of the full failure probability δ. The new sequence $\{c_t\}$ is constructed in such a way that at any time step t an element of the sequence c_t is half the width of a $1 - d_t$ confidence interval [24].

3.1.3. Base Algorithm

The base form of the empirical Bernstein stopping algorithms (EBS), called **EBStopSimple**, uses the previously introduced c_t as an upper bound an accuracy ϵ, i.e., the deviation of the empirical mean from the actual mean.
Henceforth, EBS will refer to any empirical Bernstein stopping algorithm, including modifications.
The derivations above lack a stopping condition, the goal now is to use this sequence c_t (91) to construct one. Further details can be found in the Ref. [16]. Assume that the algorithms stops at a time t if:

$$c_t \leq \epsilon(|\overline{X}_t| - c_t) \tag{92}$$

then the following also holds:

$$||\overline{X}_t| - |\mu|| \leq c_t \leq \epsilon(|\overline{X}_t| - c_t) \leq \epsilon \tag{93}$$

The equation above states that at a time t when the algorithm terminates, $|\overline{X}_t|$ will be within ϵ of μ. In the equation above one can see that if the algorithm stops at the condition in equation (92) the estimated $\overline{X}_t$ will be within a relative error ϵ of the real expected value μ. the last inequality in equation (92) results in the stopping criterion used for the EBS algorithm:

$$c_t \leq \frac{\epsilon}{1+\epsilon}|\overline{X}_t| \leq \epsilon|\overline{X}_t| \tag{94}$$

The following pseudo code algorithm uses the stopping criterion (94).

Algorithm 1 EBStopSimple

```
$c_0 \leftarrow \infty$
$t \leftarrow 1$
while $c_t > \epsilon|\overline{X}_t|$ do                    ▷ equation (94)
    Sample $X_t$
    Update $\overline{X}_t$
    Update $\overline{V}_t$
    Update $c_t$                                            ▷ equation (91)
    $t \leftarrow t + 1$
end while
$T_{\text{Stop}} \leftarrow t$                      ▷ Time at which the algorithm terminates
$\hat{\mu} \leftarrow \overline{X}_{T_{\text{Stop}}}$
return $\hat{\mu}$
```

This algorithm stops when the current expected value $\overline{X}_t$ is within ϵ of the bound c_t. Therefore, due to equation (93), the algorithm can be terminated and produce a (ϵ, δ)-estimate. To convert the algorithm 1 from relative to absolute accuracy, simply use equation (83) as the stopping condition. The algorithm 2 is an adaptation of the EBSimpleStop algorithm that Mnih [24] proposed using an absolute accuracy.

Algorithm 2 EBA

```
$c_0 \leftarrow \infty$
$t \leftarrow 1$
while $c_t > \epsilon$ do
    Sample $X_t$
    Update $\overline{X}_t$
    Update $\overline{V}_t$
    Update $c_t$                                            ▷ equation (91)
    $t \leftarrow t + 1$
end while
$T_{\text{Stop}} \leftarrow t$                      ▷ Time at which the algorithm terminates
$\hat{\mu} \leftarrow \overline{X}_{T_{\text{Stop}}}$
return $\hat{\mu}$
```

This new algorithm is called EBA, the 'A' represents for the absolute accuracy. It behaves identically to the EBStopSimple algorithm, expect that now an absolute accuracy is used.
If, for example, one estimates $\mu = 2$ and sets $\epsilon = 0.1$, the resulting absolute accuracy would be ± 0.1. Whereas the relative accuracy depends on the mean, i.e. $\epsilon|\mu| = \pm 0.2$. Importantly, a relative accuracy can cause EBS to not terminate in the case where $\mu = 0$. If $|\mu|\epsilon \to 0$ then EBS has to sample infinitely

many times to achieve an relative accuracy of ± 0, i.e. a perfect estimated, resulting in EBS not terminating.
In general, it is wasteful to check the condition of the algorithm at every time step t, this is because if the algorithm did not converge at time step a t it is unlikely that it will converge close to it. A method that uses this idea is content of the next section.

3.1.4. Modifications on EBA

Like previously mentioned, it is wasteful to check the condition every time t, because if the condition is not met after t samples, it is unlikely that it is met after $t+1$ samples. A logarithmic approach is an natural ansatz to this problem, due to the $\mathcal{O}(1/\sqrt{t})$ scaling of c_t.
The idea is to collect a number of samples in a batch and then update c_t. Collecting samples in a batch also allows the empirical variance $\overline{V}_t$ to further converge to the actual variance, leading to a tighter bound of c_t and thus a faster stopping time. To this extend Mnih *et al.* [16] introduces the variables k and t_k. Although the variable t still refers to the amount of samples that have been taken, k is the number of times c_t has been updated. The idea is to delay the update of c_t such that the batching of the samples can lead to a lower bound and therefore to earlier stopping. While there are several options of how to explicitly implement this, we only consider the so-called geometric sampling method. As mentioned above, this method batches $t_k = \lceil \beta^k \rceil$ many samples and checks the stop conditions after the k-th time. Geometric sampling checks the condition at most $\log_\beta(t)$ times, with t being the number of samples taken. Inserting $\log_\beta(t)$ into d_t (89) gives:

$$d_t = \frac{c}{t^p} \rightarrow \frac{c}{(\log_\beta(t))^p}. \tag{95}$$

Considering that c_t (see eq. (91)) is $\propto \log(1/d_t)$, a tighter bound of c_t is achieved by maximising d_t. It is clear that if $t \to \infty$ then $1/t^p < 1/\log_\beta(t)^p$, hence geometric sampling gives a tighter bound. As a consequence, the tighter bound c_t leads to earlier stopping, i.e. fewer samples for an estimate.
The bound c_t must also be modified to benefit from geometric sampling:

$$c_{t_k} = \sqrt{\frac{2\overline{V}_t \ln\left(\frac{3}{d_k}\right)}{t}} + \frac{2R\ln\left(\frac{3}{d_k}\right)}{t}. \tag{96}$$

Note that the index for d_k changed compared to equation (91), as this term is updated now with exponentially increasing gaps. Algorithm 3 below is a modification of the algorithm 2.

Algorithm 3 EBAGeo: geometric sampling

```
$t \leftarrow 1$
$k \leftarrow 0$
while $c_{t_k} < \epsilon$ do
    Sample $X_t$
    Update $\overline{X}_t$
    Update $\overline{V}_t$
    $t \leftarrow t + 1$
    if $t > \lfloor \beta^k \rfloor$ then
        $k \leftarrow k + 1$
        Update $c_{t_k}$                                  ▷ equation (96)
    end if
end while
$T_{\text{Stop}} \leftarrow t$                  ▷ Time at which the algorithm terminates
$\hat{\mu} \leftarrow \overline{X}_{T_{\text{Stop}}}$
return $\hat{\mu}$
```

Figure 8: Visual presentation of $t_k = \lceil \beta^k \rceil$. The distance between t_k and t_{k+1} becomes exponentially larger.

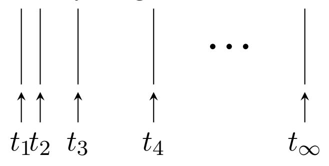

Geometric sampling introduced another parameter β which to some degree controls the stopping time of algorithm 3. Larger β tend to overshoot the lowest possible stopping time up to the extent that the proposed stopping time does not take advantage of the variance information anymore. This is because the higher k becomes the larger the difference is between $\lceil \beta^k \rceil$ and $\lceil \beta^{k+1} \rceil$. While this method reduces the stopping time, it also reduces the chance to accurately hit the smallest valid stopping time $T_{\min}$ without being off by a factor of β.
Hence, the authors, introduce a modification to this problem in Ref. [24], so-called **mid-interval sampling**. Using this modification, the algorithm checks the condition additionally in between $\lceil \beta^k \rceil + 1$ and $\lceil \beta^{k+1} \rceil$.

Algorithm 4 EBAGeoMarg: martingale-based anytime stopping

```
$t \leftarrow 1$
$k \leftarrow 0$
**while** $c_t < \epsilon$ **do**
    Sample $X_t$
    Update $\overline{X}_t$ & $\overline{V}_t$
    $t \leftarrow t + 1$
    **if** $t > \lfloor \beta^k \rfloor$ **then**
        $k \leftarrow k + 1$
        $\alpha \leftarrow \lfloor \beta^k \rfloor / \lfloor \beta^{k-1} \rfloor$
        $x \leftarrow -\alpha \ln(d_k/3)$
        $c_{tk} \leftarrow \sqrt{2\overline{V}_t x/t} + 3Rx/t$
    **end if**
**end while**
$T_{\text{Stop}} \leftarrow t$                    ▷ Time at which the algorithm terminates
$\hat{\mu} \leftarrow \overline{X}_{T_{\text{Stop}}}$
return $\hat{\mu}$
```

Furthermore, the Python implementations of the previously introduced algorithms may be found in the GitHub repository **EmpiricalBernsteinAlgorithm** [25].

3.1.5. Effect of the Variance on EBS

The empirical Bernstein stopping algorithms generally perform better in low-variance scenarios, as shown in figure 2.2.4, where the underlying bounds are compared. In order to analyse the effect of the variance, the variables ϵ, δ and the range R are kept constant while the variance is variable. One method of keeping R constant while varying the variance is to group a l random variables together, i.e., to consider their mean outcome as a new random variable. In the case of a uniformly distributed random variable, the variance of the grouped random variable thus scales with $1/l$. Let γ_l be the mean of l uniform(a, b) i.i.d. random variables X_i, i.e.

$$\gamma_l = \frac{1}{l} \sum_{i=1}^{l} X_i, \tag{97}$$

their variance then is as follows,

$$\sigma^2(\gamma_l) = \frac{(b-a)^2}{12l}. \tag{98}$$

Equation (98) shows that with increasing l, the variance is decreasing. Doing so allows us to create a benchmark of EBS while keeping ϵ, δ and the Range R constant while decreasing the variance. A benchmark of EBA, EBAGeo, EBAGeoMarg and Höffding's bound can be seen in figure 9.

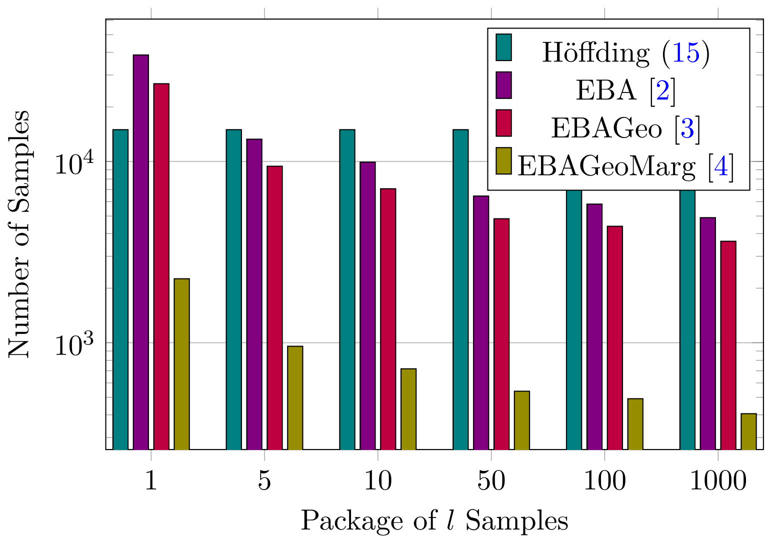

Figure 9: Effect of the variance on various sampling algorithms. Random variables are sampled from an uniform(a, b, l) distribution, with l being the number of samples that have been batched together. Each bar represents the average over 100 runs. Furthermore $\beta = 1.1$ is set for EBAGeo, while $\delta = 0.1$ and $\epsilon = 0.01$ are fixed for all algorithms. Due to eq. (98), the variance decreases with l. However, Höffding's bound is constant for a set R as it does not depend on the variance at all.

Figure 9 demonstrates how EBS needs fewer samples as the the underlying variance of the random variables gets smaller. While Höffding's bound always yields a constant amount of samples, the EBS-based algorithms leads to a decrease of the amount of samples. It is also clear that the EBAGeoMarg algorithm outperforms the other two EBS variants. Furthermore, it seems like EBAGeo overshot the actually stopping time by a factor $\approx \beta^k$, as discussed in section 3.1.4, because of the stark contrast to EBAGeoMarg.
Even though figure 9 shows a clear decrease of samples taken by the algorithms, the construction of γ_l increases the total number of samples taken by a factor of l. For a fair comparison, figure 10 shows the same bar charts as in Figure 9 but with the total number of samples taken adjusted by l accordingly. It shows how higher values of l lead to higher total number of samples taken. This is the case because the additional number of samples required to batch l samples into one is higher than EBS can save by a decreased variance by $^1/_l$.

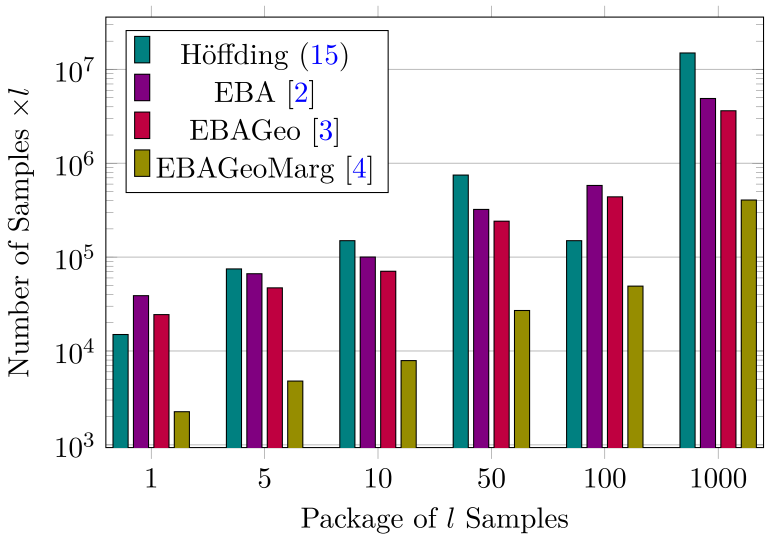

Figure 10: Data from figure 9 but adjusted to the batch size l. This represents the actual number of samples that were used. Höffding's bound does not depend on variance, it requires more samples with increased package sizes l.

3.2. Constructing a suitable VQE ansatz

An issue concerning VQE is that finding an ansatz is usually a difficult problem. When working with small numbers of qubits, one can find an ansatz by using an algorithm that decomposes an unitary matrix into a sequence of quantum gates from the universal gate set only. Such a **quantum decomposition algorithm** decomposes an unitary $2^n \times 2^n$ matrix into a sequence of X-gates and fully controlled rotational gates that act on n qubits, resulting in a circuit representation of that matrix [26]. The later form a universal set of quantum gates, which means that any unitary gate can be expressed in terms of that set of gates.
This methods will be used in section 4.1 to construct a toy example from a small Hamiltonian, for the purpose of creating benchmarks of EBA in a VQE setting. Lastly, a quick overview of how EBA will be integrated into a VQE is presented.

3.2.1. Quantum Decomposition

Let $\hat{\mathrm{U}} \in \mathbb{C}^{2n\times 2n}$ be a unitary, i.e. $\hat{\mathrm{U}}^{\dagger} = \hat{\mathrm{U}}^{-1}$, complex-valued matrix. Such a unitary $\hat{\mathrm{U}}$ can be decomposed into a combination of X-gates and fully controlled rational gates, using the quantum decomposition algorithm proposed by Fedoriaka [26]. This decomposition is computationally expensive, as it scales exponentially with the number of qubit n, i.e., $\mathcal{O}(4^n)$. A Python implementation of the this decomposition algorithm, can be accessed via the GitHub repository in Ref. [27].
For example, let

$$\hat{\mathrm{U}} = \frac{1}{\sqrt{2}} \begin{bmatrix} 1 & -1 & 0 & 0 \\ 1 & 1 & 0 & 0 \\ 0 & 0 & 1 & -1 \\ 0 & 0 & -1 & 1 \end{bmatrix}, \tag{99}$$

be a unitary matrix $\in \mathbb{C}^{4\times 4}$.
Using the decomposition algorithm on $\hat{\mathrm{U}}$ gives following circuit:

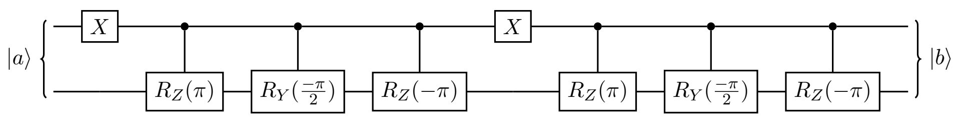

with $|a\rangle$ and $|b\rangle$ being arbitrary states $\in \mathbb{C}^4$.
The circuit above is equivalent to the equation: $\hat{\mathrm{U}}\,|a\rangle = |b\rangle$.

3.2.2. Hamiltonian to Parametrized Circuit

We want to employ an quantum circuit to find the eigenvalues of a given Hamiltonian. In the following, using quantum decomposition algorithm, we show how to design the right circuit for this task. Usually the input state for a n-qubit circuit corresponds to a bit string $b \in \{0,1\}^n$, typically the state $|0\rangle^{\otimes n}$. In order to yield the eigenvalues of th Hamiltonian, the circuit $\hat{\mathrm{U}}$ should have this basic properties:

$$\{|b\rangle\} \;—\boxed{\hat{\mathrm{U}}}\!\longrightarrow \{|\varphi\rangle\}$$

with $\{|\varphi\rangle\}$ being eigenstates of the Hamiltonian.
Now suppose a Hamiltonian $\hat{\mathrm{H}} \in \mathbb{C}^{n\times n}$. Its eigenvalue decomposition is given as:

$$\hat{\mathrm{H}} = \hat{\mathrm{U}}\Lambda\hat{\mathrm{U}}^\dagger, \tag{100}$$

with $\hat{\mathrm{U}}$ being a matrix with the eigenvectors of $\hat{\mathrm{H}}$ as its columns and Λ being matrix with its eigenvalues on its diagonal. This provides a recipe on how to obtain the eigenvalues from the quantum circuit from states corresponding to bit strings alone:

$$\lambda_i = \langle\psi_i|\,\hat{\mathrm{H}}\,|\psi_i\rangle = \underbrace{\langle\psi_i|\,\mathrm{U}}_{b\in\{0,1\}^n}\;\Lambda\;\underbrace{\mathrm{U}^\dagger\,|\psi_i\rangle}_{b\in\{0,1\}^n} \overset{!}{=} \langle b|\,\Lambda\,|b\rangle\,, \tag{101}$$

with $\{|\psi_i\rangle\}$ being an eigenstates of $\hat{\mathrm{H}}$ and $\{\lambda\}$ being the corresponding eigenvalue.
In other words, the unitary $\hat{\mathrm{U}}$ is chosen such that it maps a computational basis state $\{|b\rangle\}$, to an eigenstate $\{|\psi\rangle\}$ or $\hat{\mathrm{U}}\{|b\rangle\} = \{|\psi\rangle\}$. This unitary $\hat{\mathrm{U}}$ can be decomposed into a quantum circuit via the quantum decomposition algorithm, see sec. 3.2.1. The next step is to parameterise this circuit $\hat{\mathrm{U}}$ by adding rational gates to the circuit. While one naturally knows the optimal parameters before hand using this method, it nonetheless represents a practical ansatz.

$$\{|b_i\rangle\} \;—\boxed{\mathrm{R}(\boldsymbol{\theta})}—\boxed{\hat{\mathrm{U}}}\!\longrightarrow \{|\psi_i(\boldsymbol{\theta})\rangle\}$$

$$\{|b_i\rangle\} \;—\boxed{\hat{\mathrm{U}}(\boldsymbol{\theta})}\!\longrightarrow \{|\psi_i(\boldsymbol{\theta})\rangle\}$$

with the gate $\mathrm{R}(\boldsymbol{\theta})$ representing a black box of rotational gates acting on different qubits and $\hat{\mathrm{U}}(\boldsymbol{\theta}) := \mathrm{R}(\boldsymbol{\theta})\hat{\mathrm{U}}$.

The state $|\psi_i(\boldsymbol{\theta})\rangle$ has the energy of $\lambda_i(\boldsymbol{\theta})$. By design, there exists a set of parameters $\boldsymbol{\theta}_{\text{opt}}$ such that:

$$|\psi_i(\boldsymbol{\theta}_{\text{opt}})\rangle = \lambda_i(\boldsymbol{\theta}_{\text{opt}}) = \lambda_i. \tag{102}$$

Using these results, one can create a parameterised circuit as a circuit ansatz in order to estimate the ground state energy of the Hamiltonian. As mentioned above, this method is only feasible with small qubit numbers n, as the quantum decomposition algorithm scales exponentially with n. However, for the purpose of creating toy examples, it is satisfying to use two qubit systems.

3.2.3. EBA inside a VQE

In this thesis, our VQEs are using the gradient descent method and the SPSA method for approximating the gradient of the cost function. Hence, multiple energy measurements are required to:

- accurately estimate the ground state and
- approximate the gradient via SPSA.

For all the aforementioned energy measurements, EBA is used. More specifically, the **EBAGeoMarg** algorithm (see alg. 4) variation, as it is the best performing across all parameters choices (see section 3.1.5 and ref. [24]). A schematic overview of how the VQE will work can be see in figure 11.

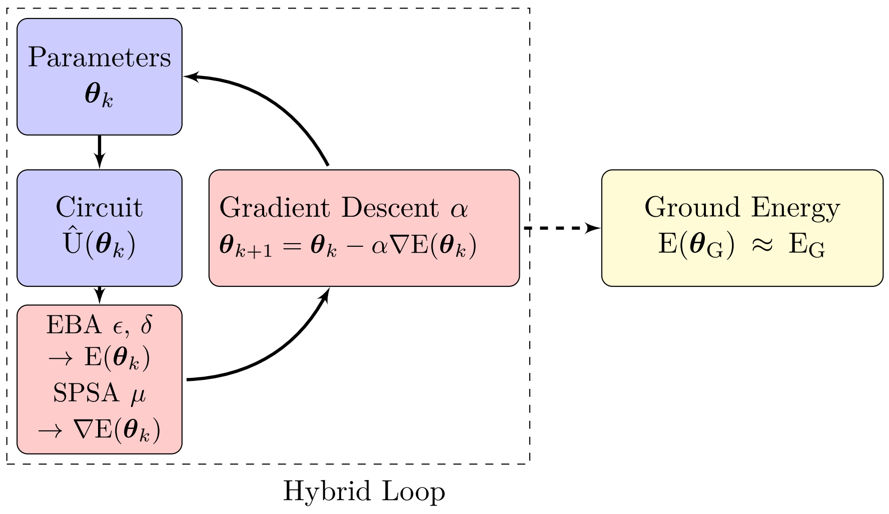
Parameters
$\boldsymbol{\theta}_k$
Circuit
$\hat{\text{U}}(\boldsymbol{\theta}_k)$
EBA ϵ, δ
$\to \text{E}(\boldsymbol{\theta}_k)$
SPSA μ
$\to \nabla\text{E}(\boldsymbol{\theta}_k)$
Gradient Descent α
$\boldsymbol{\theta}_{k+1} = \boldsymbol{\theta}_k - \alpha\nabla\text{E}(\boldsymbol{\theta}_k)$
Ground Energy
$\text{E}(\boldsymbol{\theta}_\text{G}) \approx \text{E}_\text{G}$
Hybrid Loop

Figure 11: Abbreviated version of the the flow chart 6 for a VQE. We omit the ansatz, see section 3.2. The blue boxes are part of the quantum computer while the red part is part of the classical computer. The dashed box corresponds to the hybrid loop, in which the quantum circuit and the classical optimizer work together. In each loop, the circuit provides the classical optimizer with the current energy $\text{E}(\boldsymbol{\theta}_k)$ from which it calculates the next set of parameters $\boldsymbol{\theta}_{k+1}$. The energy $\text{E}(\boldsymbol{\theta}_k)$ is estimated using EBA, while the gradient $\nabla\text{E}(\boldsymbol{\theta}_k)$ is estimated using the SPSA method. Using these measurements, the loop restarts with $\boldsymbol{\theta}_{k+1}$ which are calculated using the gradient descent method. The Yellow box shows the estimated ground energy $\text{E}(\boldsymbol{\theta}_\text{G})$. The loop is based on figure 3.

4. Results and Analysis

In the following section, the results of the benchmarks are presented. Firstly, a VQE toy example is created using the procedure from the previous section and is discussed. Based on this toy example the effect of the parameter ϵ on accuracy and the number of samples is studied. In addition to the EBA algorithm, the Höffding's bound is also used for further comparisons.
Secondly, EBA is used to estimate the ground state energy of a H_2 molecule for varying bond lengths d. This results in an energy curve for H_2 based on the distance of the two hydrogen atoms. The focus of this experiment is on reaching the necessary accuracy of these kinds of estimates.
Henceforth, we fix the EBSGeoMarg related parameters $p = 1.1$ and $\beta = 1.1$. Moreover, EBSGeoMarg [4] is the EBS algorithm of choice. Furthermore, the confidence $1 - \delta$ will not be analyzed in this thesis as one can always achieve a higher confidence by repeating the experiment [15].

4.1. Toy Example: Two Qubit System

Set the Hamiltonian:

$$\hat{\mathrm{H}} = (Z \otimes \mathbb{1}) + (\mathbb{1} \otimes X). \tag{103}$$

This explicit Hamiltonian is chosen because it acts on two qubits and is therefore small enough to be used in the quantum decomposition algorithm. Additionally, such Hamiltonian can easily be analyzed, i.e. eigenvector and eigenvalues, making it straightforward to verify results. The explicit matrix form of $\hat{\mathrm{H}}$, its eigenstates and eigenvalues, can be seen in the Appendix C. This Hamiltonian acts on two qubits and has the the eigenstates $\{|\psi\rangle\}$ with the respective eigenvalues $\{|\lambda\rangle\}$. Applying the methods of section 3.2 on $\hat{\mathrm{H}}$ or more specifically on its eigenvector matrix $\hat{\mathrm{U}}$ results in the example circuit in section 3.2.1. The parameterised circuit based on $\hat{\mathrm{U}}$ can be seen below.

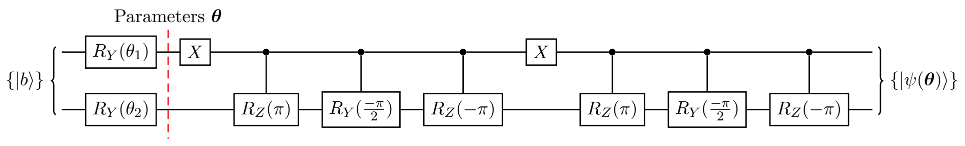

with $\boldsymbol{\theta} = (\theta_1, \theta_2)$.
This is only one of the possible ways to parameterise a circuit. Because the rotational gates have a periodicity of 4π a highly symmetric behaviour of θ_1 and θ_2 is expected. In this particular choice of parameterization, the optimal parameters are trivial to find.
Using this circuit, one can construct a VQE by simply optimizing the parameters θ_1 and θ_2.
The "ground state energy" or eigenvalue of this Hamiltonian is $E_G = -2$ with the eigenstate $|\psi_G\rangle = {}^1/\!\sqrt{2}\,\begin{pmatrix} 0 & 0 & -1 & 1^T \end{pmatrix}$ (see appendix C). This eigenstate and therefore this eigenvalue is what the VQE should converge towards. Additionally, it does not matter what bit string $\{|b\rangle\}$ is put into the parameterised circuit. Nonetheless, the state $|00\rangle$ is used as the initial state.

Visualisation of Parameterised Circuit

As the goal is to use a parameterised circuit in a VQE to find the ground state energy of a Hamiltonian $\hat{\mathrm{H}}$, it is beneficial to visualize, e.g., the expected energy as a function of the parameters. The expected energy in this case is given by, $\langle\psi(\boldsymbol{\theta})|\,\hat{\mathrm{H}}\,|\psi(\boldsymbol{\theta})\rangle$. The advantageous of having an analytically solvable Hamiltonian is that one can calculate values such as the expected value without any approximations. For instance, in the figure 12 the expected energy and variance of $\hat{\mathrm{H}}$ is displayed as a function of $\boldsymbol{\theta}$. Both the expected energy and the variance are calculated with respect to $|00\rangle$. Note the low variance regions near the minima/maxima, these are the regions in which EBS should reduce samples, while far from critical points the variance is high.

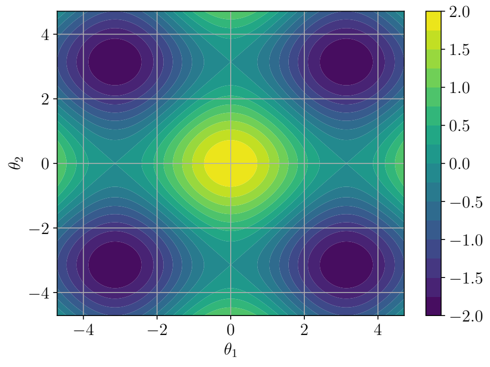

(a) Energy

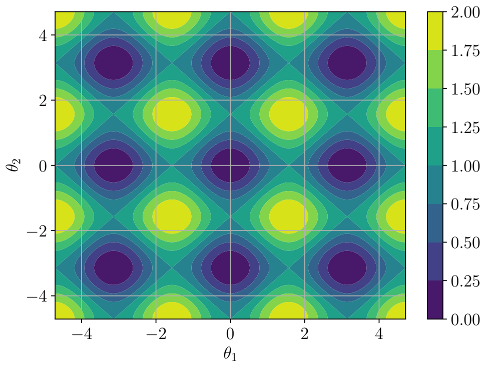

(b) Variance

Figure 12: These figures show the expected energy (a) and the variance (b) of $\hat{\mathrm{H}} = (Z \otimes \mathbb{1}) + (\mathbb{1} \otimes X)$ with respect to $\hat{\mathrm{U}}(\boldsymbol{\theta})\,|00\rangle$ as a function of the parameters $\boldsymbol{\theta} = (\theta_1, \theta_2)$. Both plots are plotted in an interval of $\boldsymbol{\theta} = [-\frac{3}{2}\pi, \frac{3}{2}\pi]$. Note that the variance is exactly zero at each minima/maxima, while being maximally in the valleys between them.

Note that gradient descent hyperparameters, i.e. the learning rate α and step size μ, do not have a drastic effect on the overall convergence of the VQE, due to the convex landscape of the chosen Hamiltonian $\hat{\mathrm{H}}$.
A run of the VQE refers to an instance of the algorithm terminating at the desired ground state energy, in this instance $E_{\mathrm{G}} = 2$. These runs consists of steps at which the algorithm measures the energy and updates the parameters according to the gradient descent algorithm, forming a path.

A collection of these runs overlaid on the underlying energy or variance landscape can be seen in the figure 13.

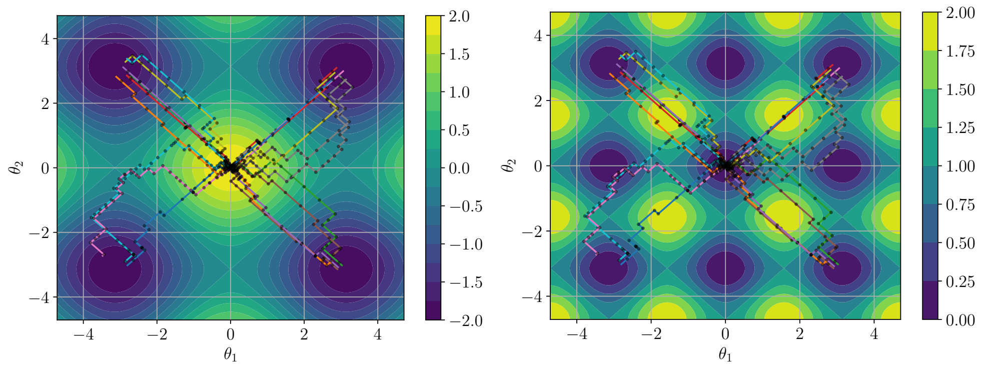

Figure 13: This figure shows the same plots as fig. 12 with multiple runs of the VQE overlaid on top. Each colour represents a different run that started at the parameters $\boldsymbol{\theta} = (0, 0)$ while the black circles represent a update step on that run. In total, there are 11 distinctive runs displayed. These runs were created using following parameters: $\alpha = 0.25$, $\mu = 0.1$, $\epsilon = 0.2$ and $\delta = 0.1$. Each run was terminated after the measured energy fulfilled the following relation for five consecutive steps: $|\hat{E} - E| \leq 0.2$. Note the seemingly random motion the path is underlying is part of the SPSA method and also that due to the high symmetric nature of the Hamiltonian each of the four surrounding minima is equally likely to be "found".

Near a minimum/maximum or saddle point the variance goes to zero causing EBS to require less samples. A figure plot of the samples required as a function of variance and distance from the origin should show symmetric behaviour due to the highly symmetric Hamiltonian. Because we are using absolute errors instead of relative error, one can calculate the minimum number of samples $n_{\min}$ (see eq.) required for an (ϵ, δ)-estimated using the Höffding bound. Note that the only variable that is depended on the specific distribution is R. One can plot this constant along with how many sample EBS needs as an comparison to a non-adaptive stopping rule.

4.1.1. Effect of ϵ on Measurement Accuracy and Confidence

The parameter ϵ has to most effect on the behaviour of EBS. Therefore, analysing it is crucial for any application of EBS. ϵ, in this case, is the absolute error or accuracy that the (ϵ, δ)-estimated of EBS will have. A lower value of ϵ, meaning higher accuracy, results in EBS requiring more samples to attain said accuracy. However in our simulation we noticed that usually EBS produces estimated with a higher accuracy than the minimum required accuracy ϵ. This can be seen in figure 14, where multiple values of ϵ are compared.

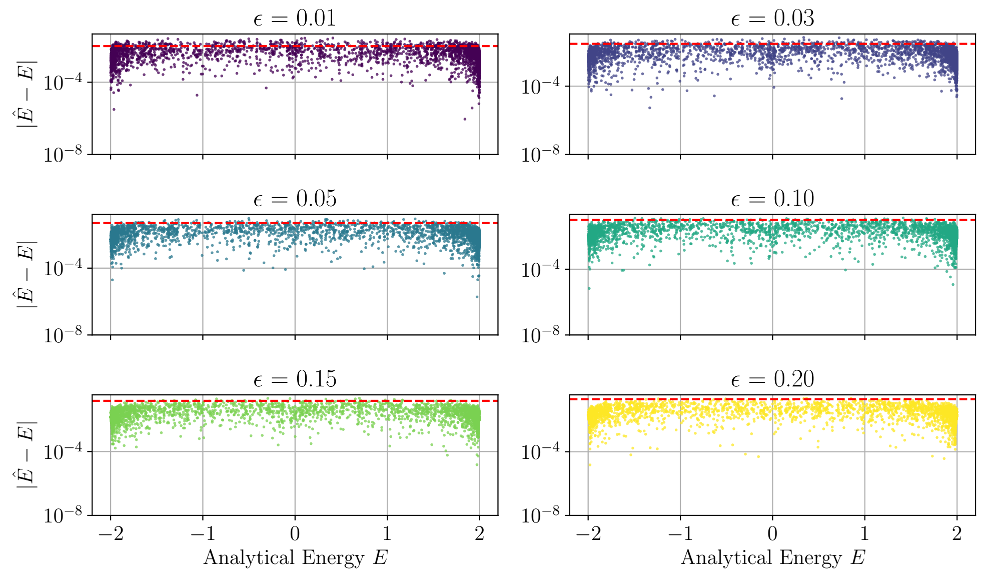

Figure 14: This figure shows the distance/ accuracy $|\hat{E} - E|$ as a function of the analytical energy E for different values of ϵ, with $\hat{E}$ being the estimated energy. The red dashed line is the corresponding value of ϵ. Each dot is a single step across different runs of the VQE. Following parameters for the VQE were used: $\alpha = 0.25$, $\mu = 0.1$ and $\delta = 0.1$. In addition with $\epsilon = \{0.01, 0.03, 0.05, 0.1, 0.1, 0.15\}$ and the EBAGeoMarg algorithm 4. Note that the actual accuracy $|\hat{E} - E|$ is usually below the set accuracy ϵ (red dashed line). While there are estimates that are above the red line, for some ϵ, this is within the set $1 - \delta$ confidence. At the eigenvalues 2 and -2 ("starting" energy and ground-state energy), the accuracy increases significantly, as the variance there is low.

The plots in figure 14 show how EBS effectively returns a higher accuracy estimated than the set accuracy of ϵ. Moreover, this effect is increased for higher values of ϵ. In addition to this higher measured accuracy $\tilde{\epsilon}$, one can see that even though the confidence probability $1 - \delta = 90\%$ is relatively high, the resulting measured confidence is significantly higher. In figure 14 only a few data energy measurements are above the red dashed line. However, these estimates that are not within ϵ of the actual energy value are well within confidence $1 - \delta$. This property of EBS is probably a result of the partitioning of the confidence δ into an interval, to ensure mathematical guarantees. The measured accuracy is below the set accuracy ϵ, besides the cases where EBS failed to produce a (ϵ, δ)-estimated. While the increased precision is a good side effect, the more relevant metric is how many samples EBS requires as a function of ϵ.
Note that the parameter δ is not compared here, as one can always achieve a higher confidence by repeating the experiment n times. This leads to an decrease of δ as estimates are deluded with more (ϵ, δ) estimates [15].

4.1.2. Effect of ϵ on Sample Complexity

Increasing the accuracy ϵ naturally requires more samples to achieve that accuracy. In settings where a certain accuracy is required but the resources are limited, i.e. quantum computing in general, reducing the amount of samples while keeping the accuracy high is crucial. A sample limit is commonly used in such scenarios; here, the sample limit is set to 10^5. However, the EBAGeoMarg algorithm did not reach this sample limit for the values chosen for ϵ in this benchmark. To visual the dependence on the variance EBA has on the amount of samples used, as a function of ϵ, the figure below is useful.

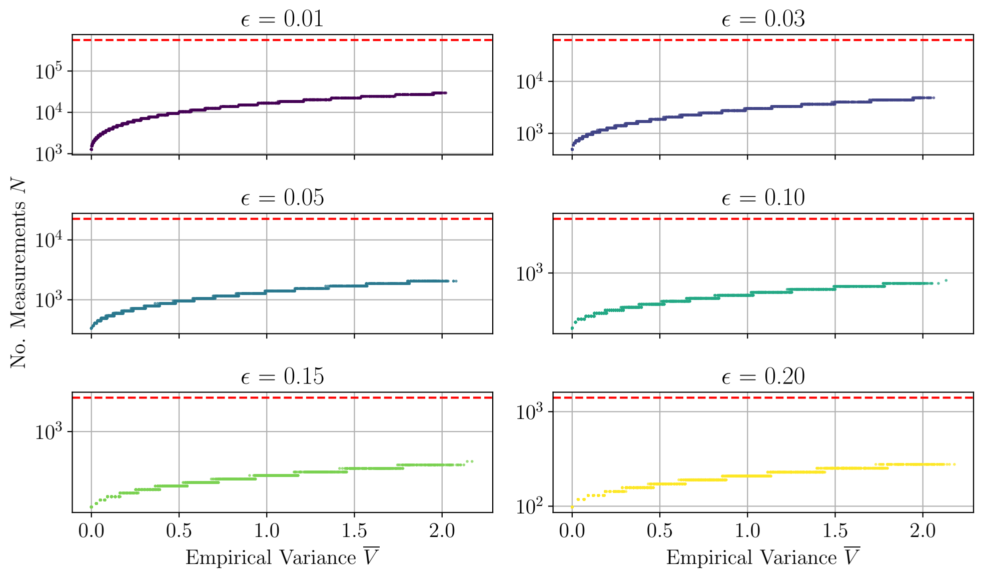

Figure 15: This figure shows the amount of samples EBS used, as a function of the estimated variance for different values of ϵ The red dashed line corresponds to t_{min} given by Höffding's bound from eq. (16). Each dot is a single step across different runs of the VQE with the same parameters. EBA required less samples than Höffding's bound across all settings of ϵ and across the whole variance spectrum. The data used in these plots are the same as in figure 14. For the EBA variation EBAGeoMarg was used, as it is the best performing.

Figure 15 shows the behaviour of EBS compared to n_{min} provided by Höffdings bound. For a set value of ϵ, δ and R, n_{min} is constant and therefore non-adaptive to the samples drawn. For a clearer picture of how ϵ influences the amount of samples for a singular run, one can plot the averaged amount of samples per run as a function of epsilon. Such a plot can be seen below.

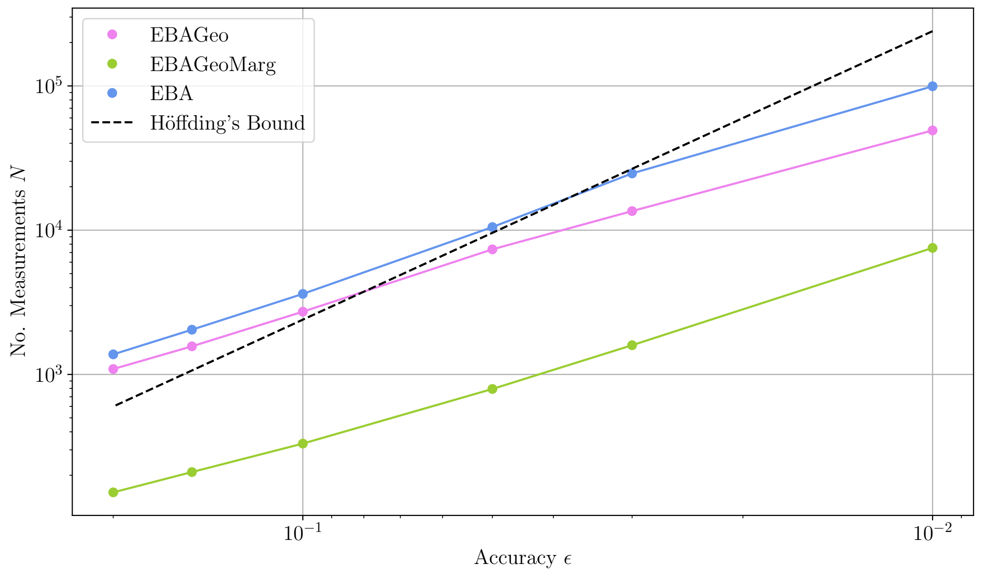

Figure 16: This figure shows the amount of samples different modification of EBS use, as a function of the accuracy ϵ. Both axes scale logarithmically. The dots are the number of measurements as given by EBA [2] (blue), by EBAGeo [3] (purple) and by EBAGeoMarg [4] (green). The dashed black line is the number of measurements given by $n_{\min}$, see. eq. (16). Each dot is averaged over 100 identical runs. The respective coloured lines (excluding dashed lines) are added for visual clarity and do not represent any data.

In the figure 16, shows a crossover point for EBA and EBAGeo but not with EBAGeoMarg. Additionally, EBAGeoMarg, being the best version of EBA, has a significantly better scaling than the EBS variations and Höffding's bound. This behaviour is expected as shown in section 3.1.5. Henceforth, only EBAGeoMarg is used when using a EBS algorithm, as it is the best performing EBS algorithm [24].

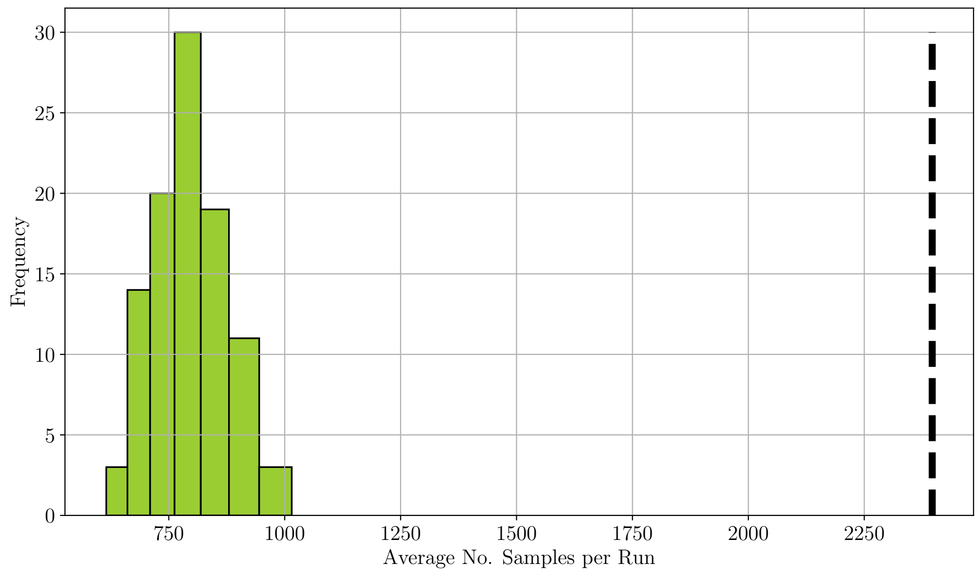

Figure 17: This figure shows a histogram of the mean number of samples per VQE run. The green data is generated using the EBAGeoMarg algorithm [4], while the dashed line represents the constant number of samples given by Höffding's bound (see eq.(16)). There are 100 runs sampled using following parameters: $\epsilon = 0.05$, $\alpha = 0.25$ and $\mu = 0.1$.

EBAGeoMarg requires significantly less samples for a single energy measurement across all variance settings and accuracy values ϵ, than the constant sample budget given by Höffding's bound. Not surprisingly figure 17 shows that EBAGeoMarg also requires less samples per run overall than Höffding's bound. The variation of the data sampled, from using EBAGeoMarg, can be partially attributed to the SPSA method that was used. The aforementioned, uses a random initialisation process to improve the gradient estimation, which then translates to randomness in the path taken. This effect can be see in figure 13. Shorter paths naturally require less samples. However, as all EBS algorithms utilise empirical variance, it is also subject to variations in energy samples.

4.1.3. Fidelity of Parameterised State

The fidelity F is measure the overlap of two states. It is defined as the modulus of the inner product of two states $|\phi\rangle$ and $|\varphi\rangle$, that is:

$$F(\psi, \varphi) = \|\langle\psi|\varphi\rangle\| \tag{104}$$

Naturally the fidelity is one if the states are the same and zero if they are orthogonal. Therefore, if the fidelity is plotted over the iterations of a VQE, it is expect to converge to 1 if the algorithm converged to the ground energy. To this extent, in the figure below, the fidelity $F(\psi_G, \psi(\boldsymbol{\theta}))$ and energy as a function of the number of iterations is plotted.

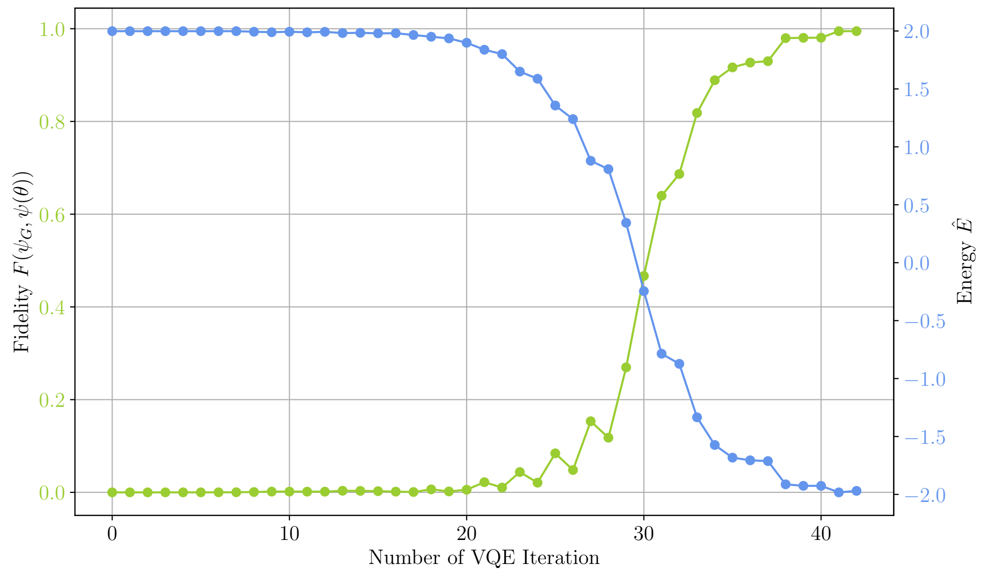

Figure 18: This figure shows a plot of the fidelity $F(\psi_G, \psi(\boldsymbol{\theta}))$ and the estimated energy $\hat{E}$ as a function of the number of iteration. A dot represents the fidelity or energy, while the lines connecting the dots are only included for visual clarity. While the Fidelity convergence to one, the energy converges to -2, i.e. the ground state energy.

In figure 18 one can see the expected behaviour of the fidelity. These plots confirm the convergence to the correct state,i.e., as $F(\psi_G, \psi(\boldsymbol{\theta}))$ converges to one, the energy converges to -2, indicating the correct estimation of the ground energy (and state). The fidelity of the state corresponding to the estimate ground energy and the actual ground state $F(\psi_G, \psi(\boldsymbol{\theta}_{opt}))$ is approximately ≈ 0.995.

4.2. Energy Curve of H_2

While the toy example from the previous section showed a proof of concept of EBS' ability to reduce the number of samples required in a VQE setting, the question is now if this holds true for more realistic and complex applications. A realistic application for a VQE is, for example, solving the electronic structure problem. The electronic structure problem looks at how the energy of a molecule depends on the specific configuration of the electrons.
In this section, we look at such a problem in the case of the H_2 molecule. The energy of the H_2 molecule depends on the bound length d, i.e. the distance between the two hydrogen atoms. The according Hamiltonian [1] is given as:

$$\hat{H} = g_1\mathbb{1} + g_2 Z_0 + g_3 Z_1 + g_4(Z_0 \otimes Z_1) + g_5(Y_0 \otimes Y_1) + g_6(X_0 \otimes X_1), \quad (105)$$

with $\{g_i\}$ being a parameter that maps to a particular bond length d. These parameters are tabulated in appendix D.
The corresponding ansatz [1] for this problem is as follows:

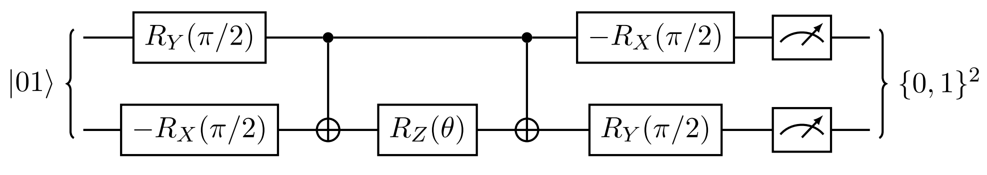

This circuit implements the unitary $\hat{\mathrm{U}}(\theta) = \exp\{-i\theta X \otimes Y\}$ as it is predicted to contain the ground state [1] of the Hamiltonian (105) .

4.2.1. VQE run for fixed d

The goal is to estimate the energy of the H_2 molecule by estimating the Hamiltonian a certain bond lengths d. To this extent, an exemplary VQE run for $d = 0.75$Å is shown first. The corresponding set of coefficients, $\{g_i\}$, can be read from appendix D

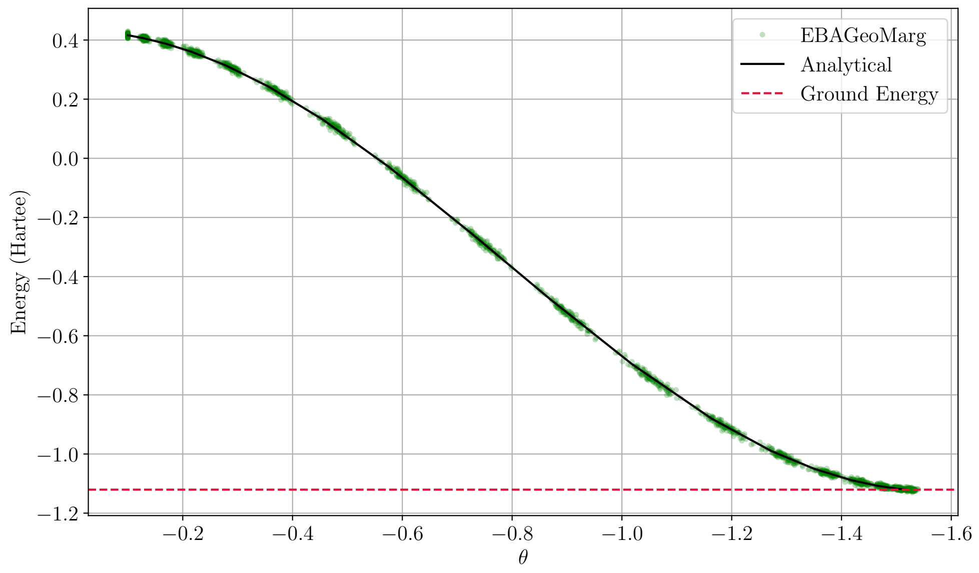

Figure 19: This figure depicts a VQE run that estimates the ground state energy of a H_2 molecule for a bond length $d = 0.75$Å, by optimising the parameter θ. The green dots are the energy estimates made with the EBAGeoMarg algorithm [4]. Additionally, the expected energy for a particular parameter θ is displayed here as a black line, while the ground energy is represented as a red dashed line. This figure represents 100 VQE runs with an initial starting parameter of $\theta_0 = -0.1$. Following parameters for the VQE are used: $\alpha = 0.1$, $\mu = 0.1$, $\epsilon = 0.01$ and $\delta = 0.1$. The measurement strategy, in this case, is to measure each non-commuting term individually and combine them to one estimate (see. sec. 4.2.2). Note that the x-axis is inverted, so that the VQE optimises towards the right.

In figure 19, the optimisation of θ can clearly be seen to converge to the ground energy. The clusters of green dots, i.e. the energy estimates, are due to the SPSA method which relies on a random initialisation process and also some variation of a energy for a certain θ is to be expected. The later is of course the case as only a finite amount of samples can be taken for an estimate. Running this VQE for an array of bond lengths d gives a energy curve of the H_2 molecule based on the bond length. However, this exemplary VQE run is first to be analysed based on accuracy ϵ in the following sections.

4.2.2. Optimal Measurement Strategy

In the section about the toy example (sec. 4.1), its Hamiltonians terms (eq. (103)) commute with each other, allowing simultaneous measurements of each term. This is generally not the case. For the H_2-VQE, the terms of Hamiltonian (eq. (105)) do not all commute. Hence, the goal is to determine what measurement strategy is the optimal one in this particular case, for EBS (and its modifications).
The straightforward method is to measure the once each in the Z, X and Y basis, and sum them up accordingly to the Hamiltonian in eq. (105) and in table 3, for a single estimate.

Table 3: Transformations for $\hat{\mathrm{H}}$ (see eq. (105))

i-th Term	$\hat{\mathrm{H}}_i$	Measurement Basis
1	$\mathbb{1}$	Offset
2	$Z_0 \otimes \mathbb{1}$	
3	$\mathbb{1} \otimes Z_1$	Z
4	$Z \otimes Z$	
5	$Y \otimes Y$	Y
6	$X \otimes X$	X

This is the case because terms $\hat{\mathrm{H}}_{2,3,4}$ do commute (bit-wise) and therefore only one measurement is done in the computational basis. For terms $\hat{\mathrm{H}}_5$ and $\hat{\mathrm{H}}_6$, one measurement each in the according basis is made. Henceforth, this method is called the naive sampler. A summary of the terms of the H_2-Hamiltonians and their respective measurement basis, can be seen in table 3. Another measurement strategy is the so-called L1 sampler, introduced by Gresch and Kliesch [28]. The L1-sampler only requires one measurement per estimate, independently of the number of Hamiltonian terms. Aforementioned, is facilitated by introducing a random sampling of the terms that are to measured, such that the term with the largest coefficient is the one most likely to be sampled and measured. However, this random process introduces a biased variance estimation, hence it is unclear if this method ultimately reduces the sample complexity when used with EBS. In general, it is unclear which measurement strategy is optimal for EBS, but in this case a quick analysis of the variance and number of measurements behaviour of these two methods will provide more insight. As can be seen in figure 20, the L1-sampler returns a biased variance estimation, compared to the unbiased estimation using the naive sampler. The effect of the variance, estimated by the L1-sampler, not converging to zero as the unbiased variance does, can be seen in the number of measurements needed for each method.

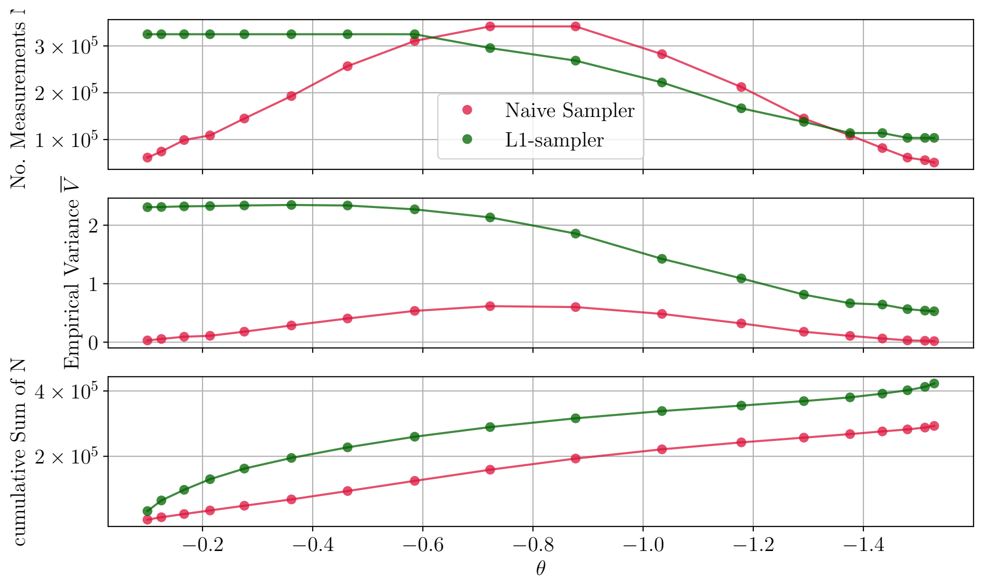

Figure 20: This plot shows the empirical variance $\overline{V}$, the number of measurements N and the cumulative sum of N, as a function of the optimisation parameter θ. The red dots (line included as visual aid) correspond to the naive sampler, while the green dots correspond to the L1-sampler. For the energy and variance estimation the EBAGeoMarg algorithm 4 was used with a respective measurement method. Following parameters for the VQE were used: $\alpha = 0.1$, $\mu = 0.1$, $\delta = 0.1$ and $\epsilon = 0.01$. Additionally, the parameters $\{g_i\}$ correspond to a bond length $d = 0.75$Å and can be seen in appendix D. Note that the x-axis is inverted, such that the VQE optimizes towards the right.

As can bee seen in figure 20, over a whole VQE optimisation run, the naive sampler requires less samples in total than the L1-sampler. While the L1-sampler required 422837 samples total, the naive sampler only required 293046 samples, resulting in a save of $\approx 31\%$. While this generally might not be the case, for this particular problem, the naive sampler is the preferable measurement strategy. Henceforth, the naive sampler is used as the measurement strategy, as it is optimal for this particular problem.

4.2.3. Effect of ϵ on Measurement Accuracy and Confidence

Quantum chemistry problems require a certain accuracy, thus the scaling of the sampling complexity based on the parameter ϵ is of importance. Similarly to section 4.1.1, the effect of accuracy ϵ on the measured accuracy and confidence is analysed. To that extent, the VQE for H_2 is run for a fixed bond length $d = 0.75$Å with variable values of ϵ.
Figure 21 shows that EBS returns an estimate below the required accuracy $1 - \delta$ of the times. Likewise to the toy example, a significantly higher accuracy than ϵ is observed. This effect is more pronounced the higher the accuracy is, or the lower ϵ is set. Further analysis on this effect is the subject of the following section. Aforementioned is to be expected, as EBS in general has overhead reserved to fulfil the guarantees of a (ϵ, δ)-estimate. Nonetheless, the confidence of δ holds as the effective confidence measured in figure 21 is

≈ 0.100. Note that the confidence $1-\delta$ is not compared here, as one can always achieve higher confidences by repeating the experiment n times. This leads to an decrease of δ as estimates are deluded with more (ϵ, δ)-estimates [15].

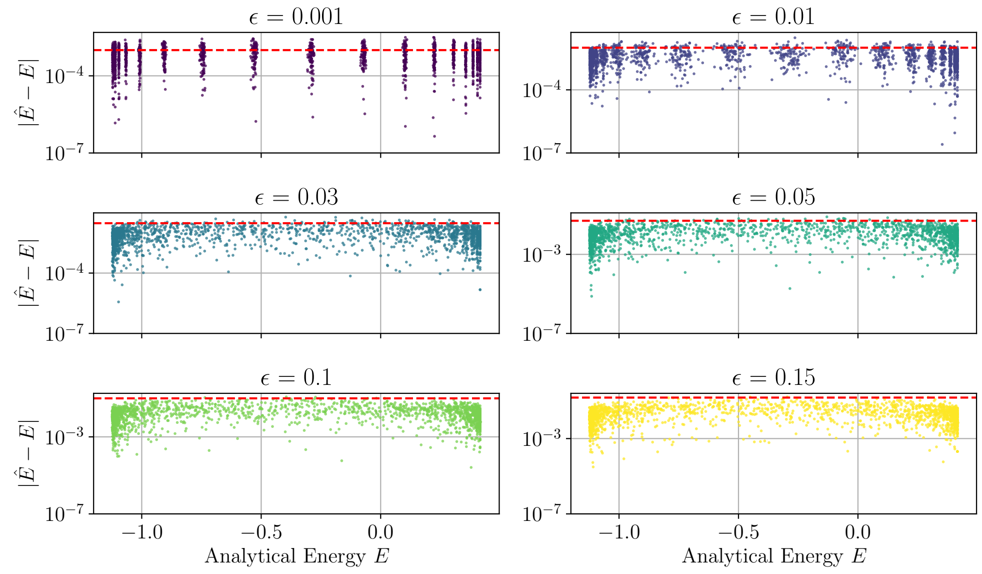

Figure 21: This figure shows the distance/ accuracy $|\hat{E} - E|$ as a function of the analytical energy E for different values of ϵ, with $\hat{E}$ being the estimated energy. The red line is the corresponding value of ϵ. Each dot is a single step across different runs of the VQE. Following parameters for the VQE were used: $\alpha = 0.1$, $\mu = 0.1$ and $\delta = 0.1$. In addition with $\epsilon = \{0.001, 0.01, 0.03, 0.05, 0.1, 0.15\}$ and the EBAGeoMarg algorithm [4]. Note that the actual accuracy $|\hat{E} - E|$ is usually below the set accuracy ϵ (red dashed line).

4.2.4. Effect of ϵ on Sample Complexity

Especially in the context of quantum chemistry the accuracy ϵ is of importance as a certain accuracy is always required for further calculations. Again, we fix the the bond length $d = 0.75$Å while varying over an array of ϵ, to analyse how EBS compares to the non-adaptive Höffding's bound.
In figure 22 the number of measurements, as given by EBS and t_{min}, can be seen as a function of the empirical variance. A similar behaviour as with the toy example in section 4.1 can be observed here. EBS required more samples in higher variance regimes but always less than the constant t_{min} provided by Höffding's bound over all variance regimes.
Additionally, an artefact of the EBAGeoMarg [4] algorithm can be seen where the number of measurements are constant for some variances. This is due to the fact that these algorithms build up an overhead that they use up before extending it.
Furthermore, for a more tangible comparison one can look at the total number of samples that are used over a VQE run in table 4. Similarly to the scaling in figure 23, for higher accuracies the difference between EBS and Höffding's is increasing. These differences, or **savings**, are significant even for the lowest values. In these settings, EBS managed to save approximately 10^4 to 10^9

samples depending on the accuracy ϵ.
Keeping in mind that in the context of actual quantum hardware, samples are a valuable resource, and minimising the amount of measurements/ samples is always of benefit. This effect is further quantified by in figure 23. The scaling of EBS (EBAGeoMarg [4]) appears to be better than of Höffding's bound, i.e. less samples for the same accuracy ϵ. This scaling behaviour is expected following the analysis of the respective bound in section 2.2.4 and ref. [24].

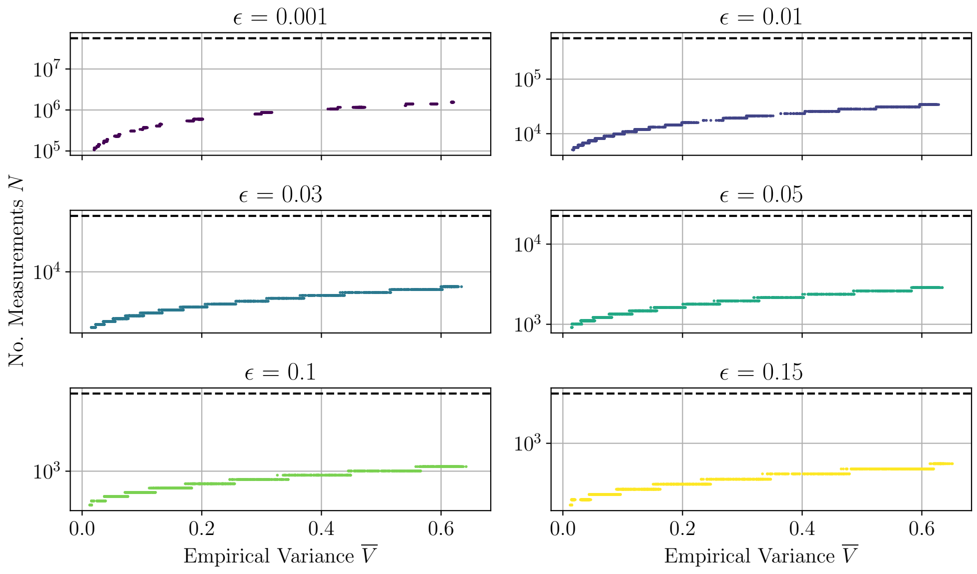

Figure 22: This figure shows the amount of samples EBS used, as a function of the estimated variance for different values of ϵ. The dashed line corresponds to $t_{\min}$ given by Höffding's bound from eq. (16). Each dot is a single step across different runs of the VQE with the same parameters. EBA required less samples than Höffding's bound across all settings of ϵ and across the whole variance spectrum. The data used in these plots is the same as in figure 21. For the EBA variation EBAGeoMarg was used, as it is the best performing. For these plots the same data as in figure 21 is used.

Table 4: Total number of samples over all variance regimes. The same data as in figure 22 used. Rounded to two decimal places. Difference is defined as total number of Höffding's bound minus EBS.

ϵ	EBS	Höffding's	Difference
0.001	1.16×10^7	1.01×10^9	1.00×10^9
0.01	2.92×10^5	1.01×10^7	9.83×10^6
0.03	6.03×10^4	1.26×10^6	1.06×10^6
0.05	3.13×10^4	4.10×10^5	3.79×10^5
0.1	1.36×10^4	1.03×10^5	8.98×10^4
0.15	8.66×10^3	4.61×10^4	3.74×10^4

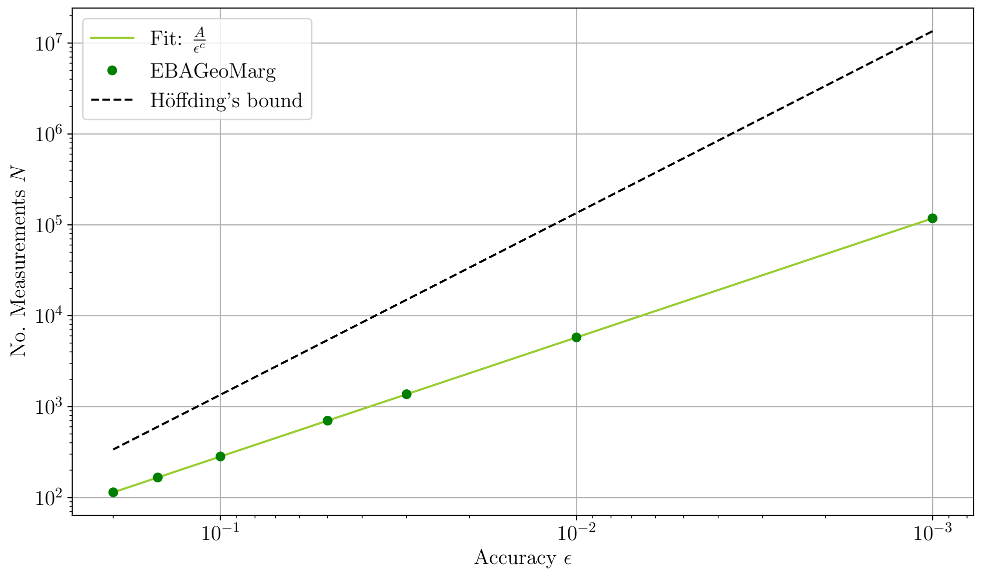

Figure 23: This figure shows a plot of the number of measurements (i.e. samples) that are required for a accuracy ϵ. Here, EBAGeoMarg [4] in red (dots) and t_{min} (16), in black (dashed line) are compared. Each data point of EBAGeoMarg, represented as a point, is averaged over 100 distinct VQE runs. Furthermore the green line is fit of the EBAGeoMarg data points, according to $\frac{A}{\epsilon^c}$ with $A = 13.83$ and $c = 1.31$. Furthermore, the x-axis is inverted so that this plot reads from left to right, i.e., the accuracy increases to the right. Note that EBAGeoMarg appears to have a better scaling for increasing accuracy, as compared to Höffding's bound. For this plot, the same data as in figure 21 is used.

4.2.5. Energy Curve of H_2

Running a VQE for an array of bond lengths d, e.g. as in section 19, gives a (total) energy curve of the H_2 molecule based on the distance of the two hydrogen atoms. Each energy measurement is made using EBS (EBAGEoMarg [4]) and therefore an accuracy of ϵ with the confidence $1 - \delta$ is guaranteed.
Such an energy curve for H_2 can be seen in figure 24. In the aforementioned figure, one notices how the number of measurements averaged over a VQE run decreases with d. This is due to the range also decreasing with d, as EBS is depending on the range (see section (19)).
Additionally, the number of iterations the VQE needs is fluctuating due to constant hyperparameters for the gradient descent and a constant starting parameter. By optimising these parameters one could achieve a reduction in measurements by virtue of shorter VQE runs. However, parameter optimisation is not the focus of this thesis.

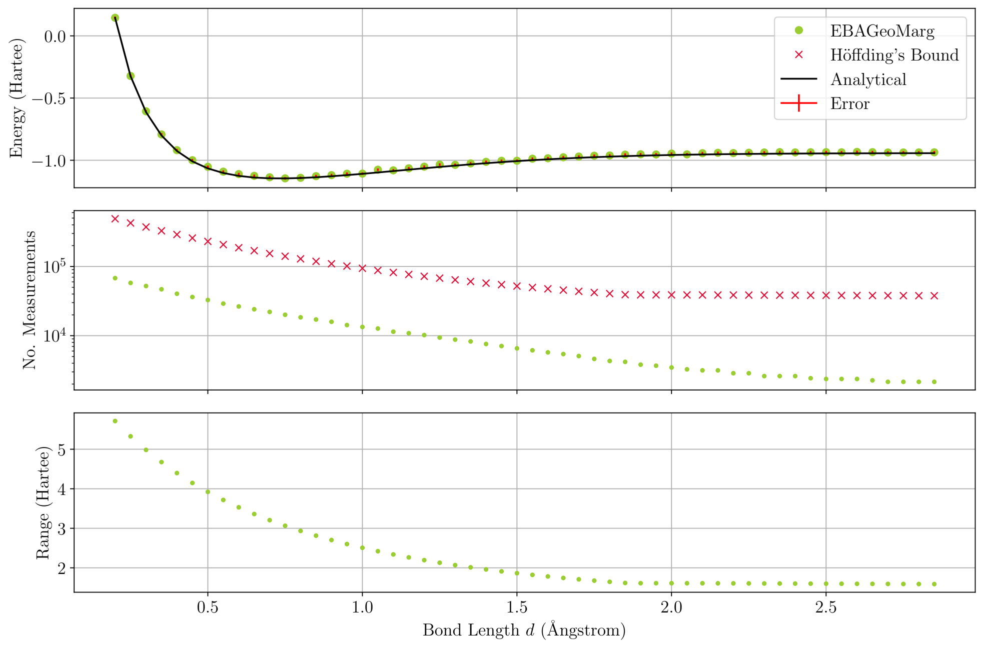

Figure 24: This plot shows the H_2 energy curve as a function of the bond length d, along side with averaged number of measurements over a VQE run and the range of the energy depending on d. The coefficients $\{g_i\}$ are tabulated in appendix D. For the energy estimation (green dots) (EBAGEoMarg [4]) is used with accuracy $\epsilon = 0.01$ and $\delta = 0.1$. The red crosses corresponds to the number of measurements given by t_{min} (see eq. 16).

Figure 24 clearly shows the scaling of EBS with the range of the energy and therefore of the samples. As the range of the samples random variables depends on the bond length d, or more specifically the corresponding parameters $\{g_i\}$, EBS requires less samples for those bond lengths. Note that despite the fact that Höffding's bound is also depended on the range and a similar downward trend can be seen, EBS provides a better bound over all d. This is to be expected as EBS performs better over all variance regimes (see figure 22).

5. Conclusion

In this thesis, we explored the use of the empirical Bernstein stopping (EBS) algorithm as a method to reduce the sample complexity in quantum computing. More specifically, EBS is used inside a VQE, where it estimated the desired ground state energy while also estimating energies at different parameters for the gradient estimation. More specifically, EBS is used to obtain energy estimates while also providing an accuracy ϵ with a confidence of $1-\delta$. This is done in the context of variations quantum algorithms (VQA), more specifically variational quantum eigensolvers (VQE), where one seeks to find the ground state of a particular Hamiltonian.
To this extend, firstly a toy example with a simple Hamiltonian was constructed using methods that decomposed this Hamiltonian into a quantum circuit. Consequently, the resulting ansatz contained the solution to our problem, i.e. the lowest eigenvalue of the Hamiltonian, as it was analytically equivalent to the Hamiltonian. EBS then was used to estimate the energy at each VQE step and additional parameters for the gradient estimation that is needed for the optimisation method used. In the case of the toy example, EBS reduced the sample complexity, i.e. reduced the number of measurements required, of the energy estimation. Surprisingly, EBS managed to outperform the non-adaptive Höffding's bound, not only across all variance regimes but also over a whole VQE optimisation run (see section 4.1.2). Additionally, in section 4.1.1, the measured accuracy matched the required accuracy ϵ with confidence $1-\delta$.
As EBS performed well above our expectations in the toy example (sec. 4.1), the next step involved an application of quantum chemistry. In this thesis, we chose to solve the electronic structure problem for the H_2 molecule using an ansatz used by O'Malley *et al.* [1]. In contrast to our constructed ansatz for the toy example, the ansatz for the H_2 molecule was a physically motivated ansatz but nevertheless just an ansatz. This problem required a closer look at the specific measurement strategy, as the Hamiltonian contained non-commuting terms that necessitated multiple measurements for a single estimate. To this extent, the L1-sampler, proposed by [28], was compared with a naive method, as it allows an energy estimation to be made using only a single measurement. The naive method proved to be more efficient in this case as the L1-sampler introduced a biased variance estimation, which significantly increased the number of measurements needed for an energy estimation.
Analysis of the sample complexity and accuracy of the estimates (section 4.2.3 & 4.2.4), again, showed that EBS did not only uphold its guarantees but also done so by utilising less measurements as compared to Höffding's bound. A tangible comparison between EBS and Höffding's bound is summarised in table 4, where the total number of samples saved by EBS clearly shows a significant improve. Using EBS for all required energy measurements, the energy curve of a hydrogen molecule, depending on the bond length d, is presented in figure 24 as the concluding result.
The conducted simulations of a hydrogen molecule and a toy example have shown the strengths of EBS and its modifications in the context of variational quantum algorithms/ eigensolvers and quantum computing in general. As measurements are an integral part of all quantum computing applications, these results are promising for other applications outside of VQAs as well.

6. Outlook

While the toy and quantum chemistry example, the electronic structure problem for H_2, showed that one can utilise the adaptive stopping algorithm EBS, to reduce the measurement effort compared to Höffding's bound. While H_2 provided a more complex and realistic problem, it is still a two qubit problem with an ansatz that is already verified to some degree. The behaviour of the variance depends on an array of variables, such as the specific ansatz and the measurement strategy. It is generally not clear which particular ansatz or measurement strategy is the optimal one for EBS. The behaviour of EBS in bigger and more complicated problems is still unclear, as the measurement strategy may influence the energy or variance estimator. However, the results for the simple problems suggest similar properties for more involved problems. Additionally, the simulation of the quantum computer for these experiments did not include noise simulation. It is again unclear how noise would influence the energy and variance estimators. More specifically it is unclear if EBS will keep its advantage over non-adaptive methods such as Höffding's bound.
The (empirical) Bernstein inequality, bound and algorithm are defined for real valued random variables, which limits its applicability for methods that deal with higher dimensional random variables. Adapting EBS for random variables beyond real valued ones, i.e. random vectors or matrices, could further improve EBS' performance, as a wide array of tools are only applicable for higher dimensional random variables.
Lastly in conjunction with the previous points, these experiments can also be repeated on actually quantum hardware. This would provide a more rounded view on how EBS deals with noise etc. .

A. Bernstein bound derivation

Let $X_1, ..., X_t$ be i.i.d random variables with range R, expected value μ and variance σ. Let $\overline{X}_t = \frac{1}{t}\sum_{i=1}^{t} X_i$ and $\Sigma^2 = \sum_{i=1}^{t}\sigma_i^2 \overset{\text{i.i.d.}}{=} t\sigma^2$.

$$\mathbb{P}[|\overline{X}_t - \mu| \geq \epsilon] \leq 2\exp\left(-\frac{(t\epsilon)^2/2}{\Sigma^2 + Rt\epsilon/3}\right) \overset{!}{=} \delta \tag{A.1}$$

The equation above can be rearranged in form more suitable for algorithms.

$$|\overline{X}_t - \mu| \geq \epsilon \tag{A.2}$$

ϵ can be calculated using the right-hand side of equation (A.1).

$$\delta = 2\exp\left(-\frac{(t\epsilon)^2/2}{t\sigma^2 + Rt\epsilon/3}\right) \tag{A.3}$$

Taking the natural log on both side and rearranging gives us:

$$\begin{aligned}\epsilon^2 &= 2\underbrace{\ln(2/\delta)}_{:=\alpha}\left(\frac{\sigma^2}{t} + \frac{R\epsilon}{3t}\right)\\ 0 &= \epsilon^2 - \frac{2R\alpha}{3t}\epsilon - \frac{2\alpha\sigma^2}{t}\end{aligned}$$

Using the binomial theorem on the equation above gives us:

$$\left(\epsilon - \frac{R\alpha}{3n}\right)^2 = \left(\frac{R\alpha}{3n}\right)^2 + \frac{2\alpha\sigma^2}{t} \tag{A.4}$$

Solving for ϵ:

$$\begin{aligned}\epsilon &= \frac{R\alpha}{3t} \pm \sqrt{\left(\frac{R\alpha}{3t}\right)^2 + \frac{2\alpha\sigma^2}{t}} \overset{!}{\geq} 0\\ \epsilon &= \frac{R\alpha}{3t} + \sqrt{\left(\frac{R\alpha}{3t}\right)^2 + \frac{2\alpha\sigma^2}{t}} \qquad\text{(A.5)}\\ &\geq \sigma\sqrt{\frac{2\ln 2/\delta}{t}} + \frac{R\ln 2/\delta}{3t} \qquad\text{(A.6)}\end{aligned}$$

Inserting the equation above into equation (A.2):

$$|\overline{X}_t - \mu| \geq \sigma\sqrt{\frac{2\ln(2/\delta)}{t}} + \frac{R\ln(2/\delta)}{3t} \tag{A.7}$$

While this looks similar to the empirical Bernstein bound (19), this equation uses the standard deviation σ not the empirical standard deviation $\overline{\sigma}_t$.

B. Quantum Mechanics/ Computing

B.1. Exponential Operator Derivation

Let $\hat{A}_{n\times n}$[7] be an operator that fulfils $\hat{A}^2 = \mathbb{1}_{n\times n}$ and $\theta \in \mathbb{R}$ then the following equation holds:

$$e^{i\theta\hat{A}} = \cos(\theta)\mathbb{1} + i\sin(\theta)\hat{A}. \tag{B.1}$$

This can be shown by expanding the exponential function with the Taylor series:

$$\begin{aligned}
e^{i\theta\hat{A}} &= \sum_{k=0}^{\infty} \frac{(i\theta\hat{A})^k}{k!} \\
&= \hat{A}^0 + i\theta\hat{A} + \frac{(i\theta\hat{A})^2}{2!} + \frac{(i\theta\hat{A})^3}{3!} + \dots \\
&= \mathbb{1} + i\theta\hat{A} - \frac{(\theta\hat{A})^2}{2!} - i\frac{(\theta\hat{A})^3}{3!} + \frac{(\theta\hat{A})^4}{4!} + \dots \\
&= \underbrace{\left(1 - \frac{\theta^2}{2!} + \frac{\theta^4}{4!} + \dots\right)}_{cos(\theta)} \mathbb{1} + i \underbrace{\left(\theta - \frac{\theta^3}{3!} + \frac{\theta^5}{5!} + \dots\right)}_{sin(\theta)} \hat{A} \\
&= \cos(\theta)\mathbb{1} + i\sin(\theta)\hat{A}.
\end{aligned} \tag{B.2}$$

B.2. Parameter Shift Rule

A method to calculate the gradient of a function is the so-called **Parameter shift rule**. It makes use of the fact that functions like equation (72) can be written in terms of sin and cos terms [29] This makes it possible to write the gradient $\nabla C(\boldsymbol{\theta}_k)$, for the k-th parameter, of a function C in terms of itself shifted in its arguments.

$$\nabla C(\boldsymbol{\theta}_k) = \frac{C(\boldsymbol{\theta}_k + \boldsymbol{\mu}_k) - C(\boldsymbol{\theta}_k - \boldsymbol{\mu}_k)}{2\sin\mu}, \tag{B.3}$$

with $\mu \neq n\pi$ and $\boldsymbol{\mu}_k = \mu\hat{e}_k$.

[7]Any square matrix $M_{n\times n}$ also fulfils this equation: $M^0_{n\times n} = \mathbb{1}_{n\times n}$

B.3. Quantum Gates

Table 5: Summary of the gates introduced in this section.

Gate	Circuit symbol	Matrix
$\mathbb{1}$	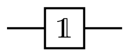	$\begin{bmatrix} 1 & 0 \\ 0 & 1 \end{bmatrix}$
X	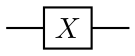	$\begin{bmatrix} 0 & 1 \\ 1 & 0 \end{bmatrix}$
Y	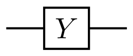	$\begin{bmatrix} 0 & -i \\ i & 0 \end{bmatrix}$
Z	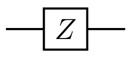	$\begin{bmatrix} 1 & 0 \\ 0 & -1 \end{bmatrix}$
H	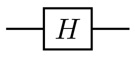	$\frac{1}{\sqrt{2}}\begin{bmatrix} 1 & 1 \\ 1 & -1 \end{bmatrix}$
CNOT	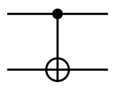	$\begin{bmatrix} 1 & 0 & 0 & 0 \\ 0 & 1 & 0 & 0 \\ 0 & 0 & 0 & 1 \\ 0 & 0 & 1 & 0 \end{bmatrix}$
$R_X(\theta)$	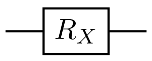	$\begin{bmatrix} \cos\left(\frac{\theta}{2}\right) & -i\sin\left(\frac{\theta}{2}\right) \\ -i\sin\left(\frac{\theta}{2}\right) & \cos\left(\frac{\theta}{2}\right) \end{bmatrix}$
$R_Y(\theta)$	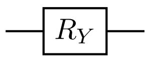	$\begin{bmatrix} \cos\left(\frac{\theta}{2}\right) & -\sin\left(\frac{\theta}{2}\right) \\ \sin\left(\frac{\theta}{2}\right) & \cos\left(\frac{\theta}{2}\right) \end{bmatrix}$
$R_Z(\theta)$	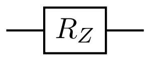	$\begin{bmatrix} e^{-i\frac{\theta}{2}} & 0 \\ 0 & e^{i\frac{\theta}{2}} \end{bmatrix}$

C. Quantum Circuit Decomposition: Example Circuit

Let $\hat{\mathrm{H}} = (Z \otimes \mathbb{1}) + (\mathbb{1} \otimes X)$. As a matrix this can be written as:

$$\hat{\mathrm{H}} = \begin{bmatrix} 1 & 1 & 0 & 0 \\ 1 & 1 & 0 & 0 \\ 0 & 0 & -1 & 1 \\ 0 & 0 & 1 & -1 \end{bmatrix} \tag{C.1}$$

The corresponding eigenstates are:

$$|\psi_1\rangle = \frac{1}{\sqrt{2}} \begin{bmatrix} 1 \\ 1 \\ 0 \\ 0 \end{bmatrix}, |\psi_2\rangle = \frac{1}{\sqrt{2}} \begin{bmatrix} -1 \\ 1 \\ 0 \\ 0 \end{bmatrix}, |\psi_3\rangle = \frac{1}{\sqrt{2}} \begin{bmatrix} 0 \\ 0 \\ 1 \\ 1 \end{bmatrix}, |\psi_4\rangle = \frac{1}{\sqrt{2}} \begin{bmatrix} 0 \\ 0 \\ -1 \\ 1 \end{bmatrix}, \tag{C.2}$$

with $\lambda_1 = 2$, $\lambda_2 = \lambda_3 = 0$ and $\lambda_4 = -2$.
Knowing the the eigenstates and the eigenvalues, the eigenvalue decomposition of $\hat{\mathrm{H}}$ is as follows:

$$\begin{aligned} \hat{\mathrm{H}} &= \hat{\mathrm{U}}\Lambda\hat{\mathrm{U}}^\dagger \\ &= \frac{1}{\sqrt{2}} \begin{bmatrix} 1 & -1 & 0 & 0 \\ 1 & 1 & 0 & 0 \\ 0 & 0 & 1 & -1 \\ 0 & 0 & -1 & 1 \end{bmatrix} \begin{bmatrix} 2 & 0 & 0 & 0 \\ 0 & 0 & 0 & 0 \\ 0 & 0 & 0 & 0 \\ 0 & 0 & 0 & -2 \end{bmatrix} \frac{1}{\sqrt{2}} \begin{bmatrix} 1 & 1 & 0 & 0 \\ -1 & 1 & 0 & 0 \\ 0 & 0 & 1 & 1 \\ 0 & 0 & -1 & 1 \end{bmatrix}. \end{aligned} \tag{C.3}$$

D. Coefficients [1] $\{g_i\}$ for eq. (105)

d	g_1	g_2	g_3	g_4	g_5	g_6
0.20	2.8489	0.5678	-1.4508	0.6799	0.0791	0.0791
0.25	2.1868	0.5449	-1.2870	0.6719	0.0798	0.0798
0.30	1.7252	0.5215	-1.1458	0.6631	0.0806	0.0806
0.35	1.3827	0.4982	-1.0226	0.6537	0.0815	0.0815
0.40	1.1182	0.4754	-0.9145	0.6438	0.0825	0.0825
0.45	0.9083	0.4534	-0.8194	0.6336	0.0835	0.0835
0.50	0.7381	0.4325	-0.7355	0.6233	0.0846	0.0846
0.55	0.5979	0.4125	-0.6612	0.6129	0.0858	0.0858
0.60	0.4808	0.3937	-0.5950	0.6025	0.0870	0.0870
0.65	0.3819	0.3760	-0.5358	0.5921	0.0883	0.0883
0.70	0.2976	0.3593	-0.4826	0.5818	0.0896	0.0896
0.75	0.2252	0.3435	-0.4347	0.5716	0.0910	0.0910
0.80	0.1626	0.3288	-0.3915	0.5616	0.0925	0.0925
0.85	0.1083	0.3149	-0.3523	0.5518	0.0939	0.0939
0.90	0.0609	0.3018	-0.3168	0.5421	0.0954	0.0954
0.95	0.0193	0.2895	-0.2845	0.5327	0.0970	0.0970
1.00	-0.0172	0.2779	-0.2550	0.5235	0.0986	0.0986
1.05	-0.0493	0.2669	-0.2282	0.5146	0.1002	0.1002
1.10	-0.0778	0.2565	-0.2036	0.5059	0.1018	0.1018
1.15	-0.1029	0.2467	-0.1810	0.4974	0.1034	0.1034
1.20	-0.1253	0.2374	-0.1603	0.4892	0.1050	0.1050

d	g_1	g_2	g_3	g_4	g_5	g_6
1.25	-0.1452	0.2286	-0.1413	0.4812	0.1067	0.1067
1.30	-0.1629	0.2203	-0.1238	0.4735	0.1083	0.1083
1.35	-0.1786	0.2123	-0.1077	0.4660	0.1100	0.1100
1.40	-0.1927	0.2048	-0.0929	0.4588	0.1116	0.1116
1.45	-0.2053	0.1976	-0.0792	0.4518	0.1133	0.1133
1.50	-0.2165	0.1908	-0.0666	0.4451	0.1149	0.1149
1.55	-0.2265	0.1843	-0.0549	0.4386	0.1165	0.1165
1.60	-0.2355	0.1782	-0.0442	0.4323	0.1181	0.1181
1.65	-0.2436	0.1723	-0.0342	0.4262	0.1196	0.1196
1.70	-0.2508	0.1667	-0.0251	0.4204	0.1211	0.1211
1.75	-0.2573	0.1615	-0.0166	0.4148	0.1226	0.1226
1.80	-0.2632	0.1565	-0.0088	0.4094	0.1241	0.1241
1.85	-0.2684	0.1517	-0.0015	0.4042	0.1256	0.1256
1.90	-0.2731	0.1472	0.0052	0.3992	0.1270	0.1270
1.95	-0.2774	0.1430	0.0114	0.3944	0.1284	0.1284
2.00	-0.2812	0.1390	0.0171	0.3898	0.1297	0.1297
2.05	-0.2847	0.1352	0.0223	0.3853	0.1310	0.1310
2.10	-0.2879	0.1316	0.0272	0.3811	0.1323	0.1323
2.15	-0.2908	0.1282	0.0317	0.3769	0.1335	0.1335
2.20	-0.2934	0.1251	0.0359	0.3730	0.1347	0.1347
2.25	-0.2958	0.1221	0.0397	0.3692	0.1359	0.1359
2.30	-0.2980	0.1193	0.0432	0.3655	0.1370	0.1370
2.35	-0.3000	0.1167	0.0465	0.3620	0.1381	0.1381
2.40	-0.3018	0.1142	0.0495	0.3586	0.1392	0.1392
2.45	-0.3035	0.1119	0.0523	0.3553	0.1402	0.1402
2.50	-0.3051	0.1098	0.0549	0.3521	0.1412	0.1412
2.55	-0.3066	0.1078	0.0572	0.3491	0.1422	0.1422
2.60	-0.3079	0.1059	0.0594	0.3461	0.1432	0.1432
2.65	-0.3092	0.1042	0.0614	0.3433	0.1441	0.1441
2.70	-0.3104	0.1026	0.0632	0.3406	0.1450	0.1450
2.75	-0.3115	0.1011	0.0649	0.3379	0.1458	0.1458
2.80	-0.3125	0.0997	0.0665	0.3354	0.1467	0.1467
2.85	-0.3135	0.0984	0.0679	0.3329	0.1475	0.1475

References

[1] P. J. O'Malley, R. Babbush, I. D. Kivlichan, J. Romero, J. R. McClean, R. Barends, J. Kelly, P. Roushan, A. Tranter, N. Ding, *et al.*, *Scalable quantum simulation of molecular energies*, Physical Review X **6**, 031007 (2016).

[2] F. Arute, K. Arya, R. Babbush, *et al.*, *Supplementary information for 'quantum supremacy using a programmable superconducting processor,'*, Nat. Int. Wkly. J. Sci **574**, 505 (2020).

[3] H.-S. Zhong, H. Wang, Y.-H. Deng, M.-C. Chen, L.-C. Peng, Y.-H. Luo, J. Qin, D. Wu, X. Ding, Y. Hu, *et al.*, *Quantum computational advantage using photons*, Science **370**, 1460 (2020).

[4] M. Cerezo, A. Arrasmith, R. Babbush, S. C. Benjamin, S. Endo, K. Fujii, J. R. McClean, K. Mitarai, X. Yuan, L. Cincio, *et al.*, *Variational quantum algorithms*, Nature Reviews Physics **3**, 625 (2021).

[5] J. R. McClean, S. Boixo, V. N. Smelyanskiy, R. Babbush, and H. Neven, *Barren plateaus in quantum neural network training landscapes*, Nature communications **9**, 4812 (2018).

[6] L. Bittel and M. Kliesch, *Training variational quantum algorithms is np-hard*, Physical review letters **127**, 120502 (2021).

[7] L. Bittel, J. Watty, and M. Kliesch, *Fast gradient estimation for variational quantum algorithms*, arXiv preprint arXiv:2210.06484 (2022).

[8] A. Peruzzo, J. McClean, P. Shadbolt, M.-H. Yung, X.-Q. Zhou, P. J. Love, A. Aspuru-Guzik, and J. L. O'Brien, *A variational eigenvalue solver on a photonic quantum processor*, Nature Communications **5**, 4213 (2014).

[9] L. Zhou, S.-T. Wang, S. Choi, H. Pichler, and M. D. Lukin, *Quantum approximate optimization algorithm: Performance, mechanism, and implementation on near-term devices*, Physical Review X **10**, 021067 (2020).

[10] H. R. Grimsley, S. E. Economou, E. Barnes, and N. J. Mayhall, *An adaptive variational algorithm for exact molecular simulations on a quantum computer*, Nature communications **10**, 3007 (2019).

[11] H. R. Grimsley, G. S. Barron, E. Barnes, S. E. Economou, and N. J. Mayhall, *Adapt-vqe is insensitive to rough parameter landscapes and barren plateaus, 2022*, URL: https://arxiv. org/abs/2204.07179. doi **10**.

[12] J. K. Blitzstein and J. Hwang, *Introduction to probability* (Crc Press Boca Raton, FL, 2015).

[13] T. Popoviciu, *Sur les équations algébriques ayant toutes leurs racines réelles*, Mathematica **9**, 20 (1935).

[14] M. Mitzenmacher and E. Upfal, *Probability and computing: Randomization and probabilistic techniques in algorithms and data analysis* (Cambridge university press, 2017).

[15] M. Kliesch, *Characterization, certification, and validation of quantum systems*, (2020).

[16] V. Mnih, C. Szepesvári, and J.-Y. Audibert, *Empirical bernstein stopping*, *Proceedings of the 25th international conference on Machine learning*, , 672 (2008).

[17] J.-Y. Audibert, R. Munos, and C. Szepesvári, *Variance estimates and exploration function in multi-armed bandit*, in *CERTIS Research Report 07–31* (2007).

[18] J. Preskill, *Quantum computing in the nisq era and beyond*, Quantum **2**, 79 (2018).

[19] M. A. Nielsen and I. L. Chuang, *Quantum computation and quantum information*, Vol. 54 (2010).

[20] Smite-Meister, *Bloch sphere, a geometrical representation of a two-level quantum system,* (2009).

[21] A. E. D. Deutsch, A. Barenco, *Universality in quantum computation*, Proceedings of the Royal Society of London. Series A: Mathematical and Physical Sciences **449**, 669 (1995).

[22] G. E. Crooks, *Gates, states, and circuits*, (2020).

[23] T. Hoffmann and D. Brown, *Gradient estimation with constant scaling for hybrid quantum machine learning*, arXiv preprint arXiv:2211.13981 (2022).

[24] V. Mnih, *Efficient stopping rules*, (2008).

[25] T. Ugur, *Empiricalbernsteinalgorithm,* (2023).

[26] V. Fedoriaka, *Decomposition of unitary matrix into quantum gates*, (2019).

[27] V. Fedoriaka, *Tool for decomposing unitary matrix into quantum gates,* (2020).

[28] A. Gresch and M. Kliesch, *Guaranteed efficient energy estimation of quantum many-body hamiltonians using shadowgrouping*, arXiv preprint arXiv:2301.03385 (2023).

[29] A. Mari, T. R. Bromley, and N. Killoran, *Estimating the gradient and higher-order derivatives on quantum hardware*, Phys. Rev. A **103**, 012405 (2021).